

Investigating the locality of neural network training dynamics.

Soham Dan*, Phanideep Gampa and Anirbit Mukherjee*

Abstract—A fundamental quest in the theory of deep-learning is to understand the properties of the trajectories in the weight space that a learning algorithm takes. One such property that had very recently been isolated is that of “local elasticity” (S_{rel}), which quantifies the propagation of influence of a sampled data point on the prediction at another data point. In this work, we perform a comprehensive study of local elasticity by providing new theoretical insights and more careful empirical evidence of this property in a variety of settings. Firstly, specific to the classification setting, we suggest a new definition of the original idea of S_{rel} . Via experiments on state-of-the-art neural networks training on SVHN, CIFAR-10 and CIFAR-100 we demonstrate how our new S_{rel} detects the property of the weight updates preferring to make changes in predictions within the same class of the sampled data. Next, we demonstrate via examples of neural nets doing regression that the original S_{rel} reveals a 2-phase behaviour : that their training proceeds via an initial elastic phase when S_{rel} changes rapidly and an eventual inelastic phase when S_{rel} remains large. Lastly, we give multiple examples of learning via gradient flows for which one can get a closed-form expression of the original S_{rel} function. By studying the plots of these derived formulas we given theoretical demonstration of some of the experimentally detected properties of S_{rel} in the regression setting.



1 INTRODUCTION

IN recent times, there has been a surge of interest in using neural networks for complex artificial intelligence tasks. Human world champions of classic hard board games have famously been defeated by neural net based approaches, [1], [2], [3], [4]. The techniques developed for such demonstrations have had deep impacts on various traditional scientific pursuits like for planning chemical syntheses, [5], drug discovery [6] and steering a quantum system towards desired dynamics [7]. All successes involve a net generalizing despite its enormous capacity and we are led to believe that this mystery is intimately tied to the dynamics of training.

In [8], [9], [10] one can see a quick survey of the myriad of hard mathematical questions that have risen from the attempts to rigorously explain the power of neural networks. A prominent recent approach towards explaining the success of deep-learning has been to try to get provable linear-time training of various kinds of neural nets when their width is a high degree polynomial in training set size, inverse accuracy and/or inverse confidence parameters (a somewhat *unrealistic* regime) [11], [12], [13], [14], [15], [16], [17], [18], [19], [20], [21], [22], [23], [24], [25]. The essential proximity of this regime to kernel methods has been elucidated separately in works like [26], [27]. Some important progress has also happened with regards to provable training of certain special finite-sized neural nets, [28], [29], [30], [31], [32], [33]. In summary, it is fair to say that the proof of convergence of neural training remains open for almost all practically relevant finitely large networks.

Separate from the above approaches of proving convergence of neural training, recent works like [34] and [35] have brought to light an exciting new feature of neural training: that it is “local”. The core phenomenon they highlighted can be framed as follows : when a neural network is being trained to classify between say, *cat* and *dog* images, then the algorithm’s weight update based on a sampled cat image significantly changes the predictions for other cat images rather than dog images and vice-versa.

While the community lacks a complete mathematical framework to capture this phenomenon, as an attempt towards that, the above papers [34] [35] did put forward the following definition of a quantity called S_{rel} - which intuitively measures the fractional change in predictions caused by a S.G.D. update at a data point \mathbf{x}' as opposed to at \mathbf{x} , when \mathbf{x} is the sampled data for computing the stochastic gradient.

Definition 1 (Defining S_{rel}). *Corresponding to a real valued hypothesis class $\mathcal{F} = \{f \mid f : \mathcal{X} \times \mathbb{R}^p \rightarrow \mathbb{R}\}$, loss function $\ell : \mathcal{F} \times \mathcal{X} \times \mathcal{Y} \rightarrow \mathbb{R}^{\geq 0}$, given any instantiation of the (possibly stochastic) training algorithm $\{\mathbf{w}_t \in \mathbb{R}^p \mid t = 1, \dots\}$ which had access to labeled data $\in \mathcal{X} \times \mathcal{Y}$ and a learning rate η , we define associated to it a family of non-negative reals valued stochastic processes, indexed by pairs of labeled input data $((\mathbf{x}, \mathbf{y}), (\mathbf{x}', \mathbf{y}'))$,*

$$\mathbb{R}^{\geq 0} \ni t \mapsto [S_{\text{rel}}(t)]_{\mathbf{x}', \mathbf{x}, \mathbf{y}} := \frac{|f(\mathbf{x}', \mathbf{w}_t^+(\mathbf{x})) - f(\mathbf{x}', \mathbf{w}_t)|}{|f(\mathbf{x}, \mathbf{w}_t^+(\mathbf{x})) - f(\mathbf{x}, \mathbf{w}_t)|} \in \mathbb{R}^{\geq 0} \quad (1)$$

where,

$$\mathbf{w}_t^+(\mathbf{x}) = \mathbf{w}_t - \eta \nabla_{\mathbf{w}_t} \ell(\mathbf{w}_t, (\mathbf{x}, \mathbf{y}))$$

• * – contributed equally. Soham Dan (sohamdan@seas.upenn.edu) is with the Department of Computer and Information Science at the University of Pennsylvania, Phanideep Gampa (gampa.phanideep.mat15@iitbhu.ac.in) is with Amazon, India and Anirbit Mukherjee (anirbit.mukherjee@manchester.ac.uk) is with The Department of Computer Science at The University of Manchester

Remark. When S_{rel} is large for many \mathbf{x}' 's spread across the data space as a response to the update \mathbf{w}_t to $\mathbf{w}_t^+(\mathbf{x})$, the predictions are changing more globally across the data space and we would call the training as being “inelastic”. And when S_{rel} is low, the training is being more “local” or “elastic”.

Remark. For a fixed choice of $((\mathbf{x}, \mathbf{y}), (\mathbf{x}', \mathbf{y}))$ the above definition will always be understood to be applicable at only those times t when $f(\mathbf{x}, \mathbf{w}_t^+(\mathbf{x})) \neq f(\mathbf{x}, \mathbf{w}_t)$ and all properties of it conjectured or proven or observed will be understood under this condition. Secondly, we shall often denote $[S_{\text{rel}}(t)]_{\mathbf{x}', \mathbf{x}, \mathbf{y}}$ as $S_{\text{rel}}(\mathbf{x}', \mathbf{x})$ or $S_{\text{rel}}(t, \mathbf{x}', \mathbf{x})$ depending on which variable dependencies we want to emphasize.

1.1 An outline of this study

A primary point of motivation of our work is to note that in the previous studies the intricate structure in the time dynamics of the above quantity was not sufficiently studied. This also leads us to propose a new definition of S_{rel} to capture the local nature of updates in neural training dynamics while learning classification tasks. We summarize our contributions in the following,

(1) In Section 1.2 we motivate and introduce a new definition of S_{rel} which is tuned to the setup of training a predictor which maps inputs to a probability distribution over a set of finite classes.

(2) In Section 1.3 we state two conjectures about S_{rel} that we posit to be capturing their importance to neural training dynamics. In Section 2 and Appendix C we give evidence towards these conjectures via experimental studies of the dynamics of S_{rel} on synthetic data and ResNet-18 training on SVHN, CIFAR-10 and CIFAR-100.

(3) In Section 1.4 we outline our theoretical results whereby we isolate certain situations of learning by gradient descent along which the time-evolution of S_{rel} (Definition 1) can be exactly calculated. The structure of these closed form expressions give evidence towards some of the conjectures above. The corresponding formal theorem statements and full proofs are given through Sections 3, 4 and 5 and Appendices A and B

1.2 A new definition of local elasticity specifically for classification tasks.

Definition 2 (Defining S_{rel} for probability simplex valued predictors). Suppose $\mathbf{g}_{\mathbf{w}} : \mathbb{R}^n \rightarrow \mathbb{R}^C$ is a probability simplex valued predictor i.e $\mathbf{g}_{\mathbf{w}}(\mathbf{x})_i \in [0, 1]$, $\sum_{i=1}^C \mathbf{g}_{\mathbf{w}}(\mathbf{x})_i = 1 \ \forall \mathbf{x} \in \mathbb{R}^n$, $\forall i \in \{1, \dots, C\}$

$$\begin{aligned} \mathbb{R}^{\geq 0} \ni t \mapsto S_{\text{rel}}(t, \mathbf{x}', \mathbf{x}) &:= [S_{\text{rel}}(t)]_{\mathbf{x}', \mathbf{x}, \mathbf{y}} \\ &:= \frac{\text{KL}(\mathbf{g}(\mathbf{x}', \mathbf{w}_t^+(\mathbf{x})), \mathbf{g}(\mathbf{x}', \mathbf{w}_t))}{\text{KL}(\mathbf{g}(\mathbf{x}, \mathbf{w}_t^+(\mathbf{x})), \mathbf{g}(\mathbf{x}, \mathbf{w}_t))} \in \mathbb{R}^{\geq 0} \end{aligned}$$

where

$$\mathbf{w}_t^+(\mathbf{x}) = \mathbf{w}_t - \eta \cdot \nabla_{\mathbf{w}_t} \ell(\mathbf{w}_t, (\mathbf{x}, \mathbf{y}))$$

Note that in the definition above the output of \mathbf{g} is always a probability vector and we recall that given two probability vectors $\mathbf{p}, \mathbf{q} \in [0, 1]^C$ s.t $\sum_{i=1}^C p_i = 1 = \sum_{i=1}^C q_i$, we have, $\text{KL}(\mathbf{p}, \mathbf{q}) = \sum_{i=1}^C p_i \log \left(\frac{p_i}{q_i} \right)$

A natural use-case of the above definition is when studying the training of a network f_{NN} (parametrized by weight vector \mathbf{w}) composed with a layer of soft-max, i.e., the mapping $\mathbf{g}_{\mathbf{w}} := \text{Soft-Max} \circ f_{\text{NN}} : \mathbb{R}^n \rightarrow \mathbb{R}^C$. This composed function $\mathbf{g}_{\mathbf{w}}$ would commonly be trained via the cross-entropy loss $\ell = \ell_{\text{CE}}$ on a C class labelled data.

Further, we would like to note that Definition 1 focused on the changes in the predictor’s output. In contrast our proposed Definition 2, tuned to the classification setup, is trying to capture the ratio between the change in the predicted distribution over the classes at the test point \mathbf{x}' and the corresponding change in the predicted distribution over the classes at the sampled point \mathbf{x} .

We posit that its more useful to make the new S_{rel} more sensitive to the class identities rather than to the specific members of the class being sampled in a given update. Towards that we define the following smoothened version of S_{rel} adapted to the classification setting,

Definition 3 (Defining smoothened S_{rel} for probability simplex valued predictors). Given the setup as in Definition 2, we further define the following smoothened quantity corresponding to any choice of $2k$ data points $\{\mathbf{x}_{c_1, i} \mid i = 1, \dots, k\}$ and $\{\mathbf{x}_{c_2, i} \mid i = 1, \dots, k\}$ from any two classes c_1 and c_2 respectively.

$$\begin{aligned} S_{\text{rel}}^{k, \text{smooth}}(t, \{\mathbf{x}_{c_1, i}, \mathbf{x}_{c_2, i} \mid i = 1, \dots, k\}) \\ &:= \frac{\sum_{i=1}^k \sum_{j=1}^k S_{\text{rel}}(t, x_{c_1, i}, x_{c_2, j})}{k^2} \end{aligned} \quad (2)$$

In the later sections, we will use the above smoothened version of Definition 2 when investigating classification experiments.

1.3 Conjectures about S_{rel} (Definitions 1 and 3)

Towards framing the conjectures, we focus on Definition 1 and we propose to understand this S_{rel} by identifying learning processes where the following two properties of it can be established,

Firstly, that there exists a *time-independent* fairness/“unrelatedness” condition on the pair of points \mathbf{x} and \mathbf{x}' which if true would imply that $[S_{\text{rel}}(t)]_{\mathbf{x}', \mathbf{x}, \mathbf{y}}$ is small.

Secondly, that the learning process shows at least 2 phases : an initial phase when the “elastic” i.e for any pair of points $(\mathbf{x}, \mathbf{x}')$ s.t $\mathbf{x} \neq \mathbf{x}'$, S_{rel} is very small i.e the induced change in prediction at \mathbf{x}' by virtue of an S.G.D. update made via sampling the data at \mathbf{x} is only a very small fraction of the change induced in the prediction at \mathbf{x} by virtue of the same update. Recall that this is a “fictitious” update since the actual algorithm could be anything else (like gradient flow

as in our later sections) and not necessarily S.G.D. with mini-batch 1 as imagined by the quantity $w_t^+(\mathbf{x})$ which enters the definition of S_{rel} .

And there would be another late phase when the training is “inelastic” i.e. $[S_{\text{rel}}(t)]_{\mathbf{x}', \mathbf{x}, \mathbf{y}} > C(t, \mathbf{x}, \mathbf{x}') > 0$ for some function C with a sufficiently high lowerbound.

Experiments further reveal that (a) during the initial elastic phase, $S_{\text{rel}}(t)$ is a rapidly increasing function of time while in the late phase its not. And (b) that at all times - hence during both the above phases - $[S_{\text{rel}}(t)]_{\mathbf{x}', \mathbf{x}, \mathbf{y}}$ is larger for \mathbf{x} and \mathbf{x}' which are nearer. *Thus the influence of the sampled data maintains the local nature of its influence at all times.*

Although we do not yet know the precise class of learning algorithms where the above two properties hold, based on the studies to be presented in this work, we make the following two conjectures quantifying the above ideas,

Conjecture 1.1 (Distance-like functions on the data space which bound S_{rel}). \exists learning situations as described in the setup of Definition 1 with $\mathcal{X} = \mathbb{R}^n$ s.t,

- \exists a time $\tilde{t} > 0$ and a metric g on the data space s.t for any given \mathbf{x}' and \mathbf{x}_h , $\exists \mathbf{x}_\ell$ s.t $g(\mathbf{x}', \mathbf{x}_\ell) < g(\mathbf{x}', \mathbf{x}_h)$ and $S_{\text{rel}}(\mathbf{x}', \mathbf{x}_\ell) > S_{\text{rel}}(\mathbf{x}', \mathbf{x}_h)$.
- There exists a function $\mathbf{P} : \mathbb{R}^n \times \mathbb{R}^n \rightarrow [0, \infty)$ which is symmetric in its inputs s.t, $S_{\text{rel}}(\mathbf{x}, \mathbf{x}') = \mathcal{O}(\mathbf{P}(\mathbf{x}, \mathbf{x}'))$

Note that the first part of the above conjecture does not rule out that for any time t the graph of $[S_{\text{rel}}(t)]_{\mathbf{x}', \mathbf{x}, \mathbf{y}}$ vs $g(\mathbf{x}', \mathbf{x})$ won't have any local maxima. Rather it says that this plot will have a downward trend in general. In other words, for all times after \tilde{t} the influence of the prediction at \mathbf{x}' of an update based on sampling \mathbf{x} , diminishes without too many abrupt changes as \mathbf{x} gets farther away from \mathbf{x}' in the metric g . We also note that the first part of the above conjecture is asymmetric in \mathbf{x} and \mathbf{x}' . Further, the function \mathbf{P} conjectured to exist in the second part gives a *time-independent* proximity/“relatedness” condition on the pair $(\mathbf{x}, \mathbf{x}')$ for $S_{\text{rel}}(\mathbf{x}, \mathbf{x}')$ to be low - and this is a priori different from g .

Conjecture 1.2 (A 2-phase behaviour in time is seen by S_{rel}). We continue in the same setup as in Conjecture 1.1.

- **(Early times)** \exists time instants $0 \leq t_1 < t_2 < t_* < \infty$ s.t $\forall (\mathbf{x}, \mathbf{x}') S_{\text{rel}}(\mathbf{x}, \mathbf{x}')$ in the time interval $[t_1, t_2]$ is smaller than any value it attains for $t \geq t_*$.
- **(Late times)** $\forall (\mathbf{x}, \mathbf{x}'), \forall t \in [t_*, \infty), S_{\text{rel}}(\mathbf{x}, \mathbf{x}') > C(t, \mathbf{x}, \mathbf{x}') > 0$ for a function $C : \mathbb{R} \times \mathbb{R}^n \times \mathbb{R}^n \rightarrow (0, \infty)$ which is non-decreasing in its t -dependence.

Just as the late time lowerbound $C(t, \mathbf{x}, \mathbf{x}')$ is expected to have a non-trivial dependence on $(\mathbf{x}, \mathbf{x}')$, similarly the range of values attained by $S_{\text{rel}}(\mathbf{x}, \mathbf{x}')$ in the early times, $[t_1, t_2]$, is also expected to have a strong dependence on the data pair $(\mathbf{x}, \mathbf{x}')$. We anticipate that there exists proximity conditions on the pair $(\mathbf{x}, \mathbf{x}')$ which if true/false then it would consequentially raise/lower the value of $S_{\text{rel}}(\mathbf{x}, \mathbf{x}')$

for $t \in [t_1, t_2]$ and also the value of $C(t, \mathbf{x}, \mathbf{x}')$ for all $t > t_*$ - while still maintaining the distinction between the early time (before t_*) and late time (after t_*) behaviour.

Hence in words, we conjecture that neural regression is characterized by a time scale t_* about which they undergo a “phase transition” - that compared to the early times, they behave “less elastically” in the later stages of the process.

Finally, informally we note here as to what we see as to be the consistent behaviour for the extended idea of $S_{\text{rel}}(t)^{k, \text{smooth}}$ as given in Definition 3 - recalling that c_2 is the class from which the fictitious S.G.D. update sampled the data, we expect that for $c_1 = c_2$ i.e. $S_{\text{rel}}(t)^{k, \text{smooth}}$ considered intra-class, is fairly time independent and $S_{\text{rel}}(t)^{k, \text{smooth}}$ is always smaller when the two classes are different.

Thus $S_{\text{rel}}(t)^{k, \text{smooth}}$ quantifies how local to the true class of the sampled data are the changes that the algorithms make to the predictor while doing classification.

1.3.1 Experimental evidence for the above conjectures

In Sections 2.1 and 2.2 we give experimental evidence for the conjectures about the S_{rel} as in Definition 3 and similarly in Section 2.3, corresponding to Definition 1.

1.4 A Summary of Our Theoretical Results About S_{rel} (Definition 1)

We isolate three models of learning by integrable gradient flows and along their solutions we give closed-form expressions for the time evolution of S_{rel} as given in Definition 1. When the structure of these closed-form expressions are studied, they are seen to give evidence for many of the conjectured behaviour of S_{rel} on nets.

Firstly, in Section 3 we consider a model of training the last layer of a neural net. Here we show that the gradient flow on a penalized regression over features with *discrete labels* is exactly integrable. We use this to derive a closed-form expression for S_{rel} for this model and plot its dynamics for synthetic classification data.

Next, we move on to consider S_{rel} for two exactly solvable gradient flow models of regression with *continuous labels*.

In Section 4 we analyze learning of a ReLU gate, a situation where the predictor function is not a polynomial in the weights. Finally in Section 5 we analyze a situation where the predictor functions being trained are polynomial in their parameters/“weights”.

Model	Result	Conjecture that it evidences	Example of Exact S_{rel}
Classification by features	Theorem 3.2	Conjecture 1.2 (later part)	Theorem 3.2
A single ReLU gate	Lemma 4.3	Conjecture 1.2 (later part)	(implicitly contained in the discussion)
Weight d -homogeneous feature linear predictors	Theorem 5.1 Theorem 5.3	Conjecture 1.1 (later part) Conjecture 1.2 (later part)	Theorem 5.2

1.4.0.1 We note the following salient points about the above, (a) In each of the above cases we get a closed form expression for S_{rel} without having to make any specific distributional choice for the data beyond realizability. (b) The plots of these exact S_{rel} formulas evidence the first part of both the above conjectures. In particular the plots of the dynamics immediately reveal a two phase behaviour of training : an initial elastic phase when S_{rel} changes rapidly and an eventual inelastic phase when S_{rel} remains larger than during initial times. (c) Lastly, we emphasize that for the above models, the theoretical prediction closely matches time evolution of the S_{rel} evaluated on S.G.D. in the same scenario.:

2 EXPERIMENTAL STUDY OF THE TIME DYNAMICS OF S_{rel}

We will first present a thorough empirical study of the time dynamics of S_{rel} using our newly proposed Definition 3 for the benchmark classification tasks on the datasets: SVHN [36], CIFAR-10 and CIFAR-100¹.

2.1 A Study of Smoothed S_{rel} (Definition 3) on SVHN

SVHN [36] is a real-world image classification dataset that is similar in flavor to MNIST but incorporates more labeled data which comes from a significantly harder, unsolved, real world problem of recognizing digits and numbers in natural scene images. SVHN is obtained from house numbers in Google Street View images and it consists of 73257 digits for training and 26032 digits for testing.

For this experiment we train a ResNet-18 architecture, composed with a soft-max layer using the cross-entropy loss, on the SVHN training data and identify the top-3 classes with the highest class-wise accuracy. We then train a new ResNet-18 model², again with softmax and the cross-entropy loss, on these top-3 classes. We choose $k = 20$ training data from each class and track the smoothed version of S_{rel} i.e $S_{\text{rel}}^{k, \text{smooth}}$ as given in Definition 3 for all the 9 possible class

pairs. Some further details of the experimental setup are as follows in the table,

Parameter	Value
Depth of ResNet	18 (no batch norm)
The map that the f_{NN} implements	$\mathbb{R}^{3 \times 32 \times 32} \rightarrow \mathbb{R}^{10}$
Optimizer	ADAM
Learning rate	$1 \cdot 10^{-4}$
Mini-batch size	250
Dropout or any other regularization	Not Used
Top 3 classes for SVHN	0,2,4

In Figure 1, we see the time evolution of smoothed S_{rel} for all the 9 possible class pairs corresponding to images from the classes, $\{0, 2, 4\}$. The plots show the mean S_{rel} value (averaged over 5 random runs) for each class pair as well as the standard deviation. We observe that for all pairs, the intra-class S_{rel} value is higher than the inter-class S_{rel} value. Further, while the intra-class S_{rel} value remains relatively constant through the training process, the inter-class S_{rel} value progressively decreases as training progresses.

2.2 A Study of Smoothed S_{rel} (Definition 3) on CIFAR-10

CIFAR-10 [37] is a labeled subset of the 80 million tiny images dataset. It consists of 10 mutually exclusive classes containing different animals and vehicles. It has 50,000 training images and 10,000 test images.

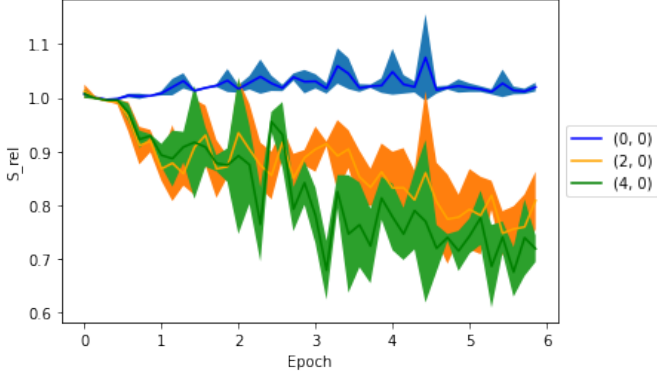
For this experiment we train a ResNet-18 architecture, composed with a soft-max layer using the cross-entropy loss, on the CIFAR-10 training data and identify the top-3 classes with the highest class-wise accuracy. We then train a new ResNet-18 model³, again with softmax and the cross-entropy loss, on these top-3 classes. We choose $k = 20$ training data from each class and track $S_{\text{rel}}^{k, \text{smooth}}$ as given in Definition 3 for all the 9 possible class pairs. Some further details of the experimental setup are as follows in the table,

Parameter	Value
Depth of ResNet	18 (no batch norm)
The map that the f_{NN} implements	$\mathbb{R}^{3 \times 32 \times 32} \rightarrow \mathbb{R}^{10}$
Optimizer	ADAM
Learning rate	$1 \cdot 10^{-4}$
Mini-batch size	250
Dropout or any other regularization	Not Used
Top 3 classes for CIFAR-10	plane, car, ship

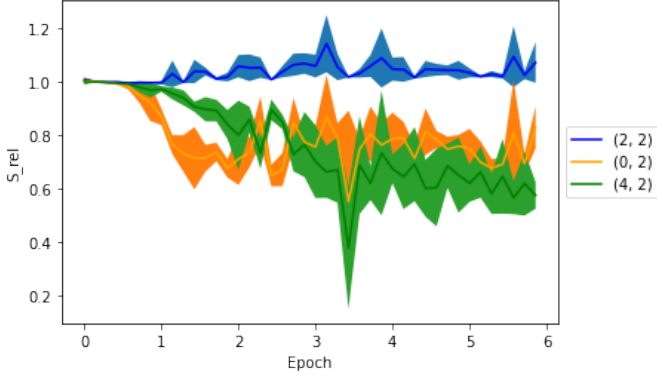
In Figure 2 we see the time evolution of smoothed S_{rel} for all the 9 possible class pairs corresponding to images from the classes, $\{\text{plane}, \text{car}, \text{ship}\}$. The plots show the mean S_{rel} value (averaged over 5 random runs) for each class pair as well as the standard deviation. Again, we observe that for all pairs, the intra-class S_{rel} value is higher than the inter-class S_{rel} value and, while the intra-class S_{rel} value remains relatively constant through the training process, the inter-class S_{rel} value progressively decreases as training progresses.

1. The CIFAR-100 results are presented in the Appendix C
2. For the experiments in this section we remove batch-normalization from the ResNet-18 model, so as to facilitate defining gradient updates with mini-batch size 1 which is necessary to define \mathbf{w}_t^+ in Definition 2 and Definition 3.

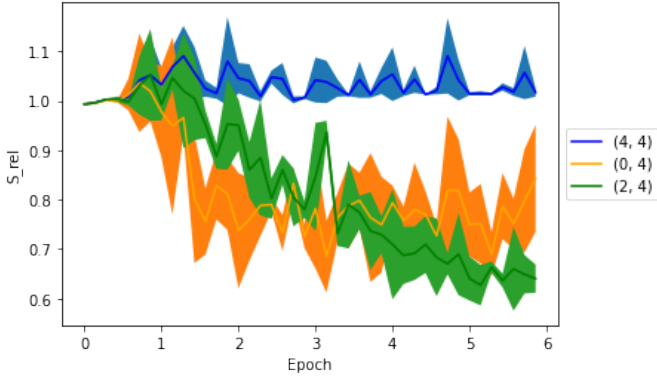
3. Again, we remove batch-normalization from the ResNet-18 model, for gradient updates with mini-batch size 1 which is necessary to define \mathbf{w}_t^+ in Definition 2 and Definition 3.



(a)



(b)



(c)

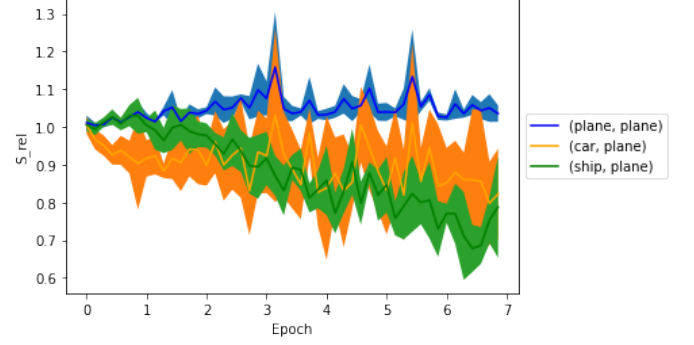
Fig. 1. $S_{\text{rel}}^{\text{smooth}}$'s time evolution for the two image classes being chosen from $\{0, 2, 4\}$ with Class- x being 0 in (a), 2 in (b) and 4 in (c)

2.3 A Study of S_{rel} (Definition 1) for Regression on Non-Realizable Data

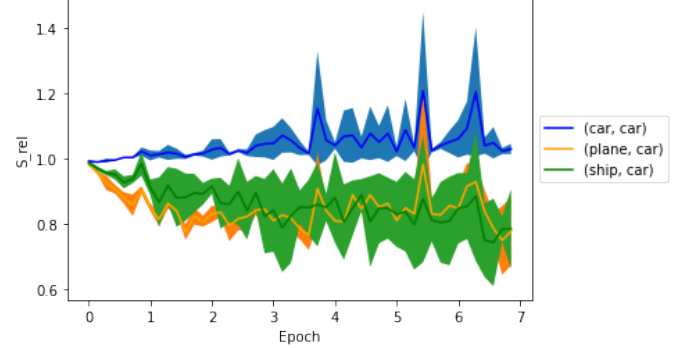
In here we will do an empirical study of the time evolution of S_{rel} as in Definition 1 for a regression problem over synthetic data with deep nets.

In the experiments here we consider doing regression using feed-forward neural networks over an instance of non-realizable data, i.e, we construct the data (\mathbf{x}, y) s.t \mathbf{x} is sampled from a standard normal distribution and $y = \|\mathbf{x}\|_1$.

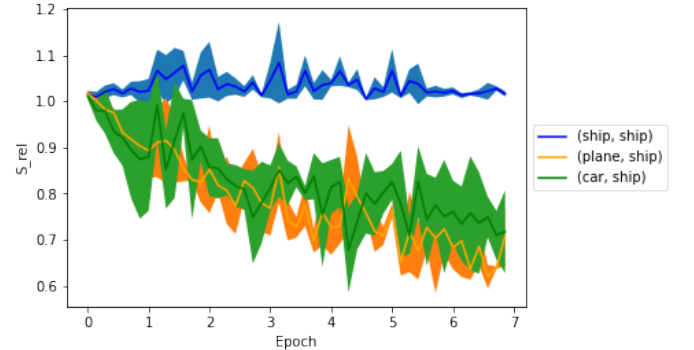
We choose the architecture and the hyper-parameters of the experiment as listed below,



(a)



(b)



(c)

Fig. 2. $S_{\text{rel}}^{\text{smooth}}$'s time evolution for the two image classes being chosen from $\{\text{plane}, \text{car}, \text{ship}\}$ with Class- x being plane in (a), car in (b) and ship in (c)

Parameter	Value
Depth of the net	5
The (uniform) width of the net	90
The map that the net implements	$\mathbb{R}^{50} \rightarrow \mathbb{R}$
Training set size	16000
Test set size	4000
Optimizer	ADAM
Learning rate	$1 \cdot 10^{-4}$
Mini-batch size	128
Dropout or any other regularization	Not Used

We demonstrate the following plots for the above experiment,

- In Figure 3 for a fixed \mathbf{x}' we choose many different values of \mathbf{x}_i and plot $S_{\text{rel}}(t, \mathbf{x}', \mathbf{x}_i)$ vs $\|\mathbf{x}' - \mathbf{x}_i\|$. We do this plot at different $t = 100, 200, 400, 800, 1600, 2400$

and show how the trends as proposed in Conjecture 1.1 happen at all times.

- In Figure 4 we choose two pairs of $(\mathbf{x}, \mathbf{x}')$ from the above with their $\|\mathbf{x}' - \mathbf{x}\|_2$ being different. Then we plot the mean value of $S_{\text{rel}}(t, \mathbf{x}', \mathbf{x})$ vs t for each of these pairs for $t = 1, \dots, 2500$, averaged over 5 random runs. We also show the variance of the values for each pair via the width of the shaded areas. Thus here we see that Conjecture 1.2 bears out.
- In Figure 5 we show the above plot overlaid against how the population and the empirical risks fall with time. From here we realize that the initial rising part of $S_{\text{rel}}(t)$ for any choice of $(\mathbf{x}, \mathbf{x}')$ coincides with the phase of training when both the risks are falling rapidly.

Figures 3 and 4 are the plots many of whose key features will be seen to be reproduced in the theoretical model to be presented in Section 5.

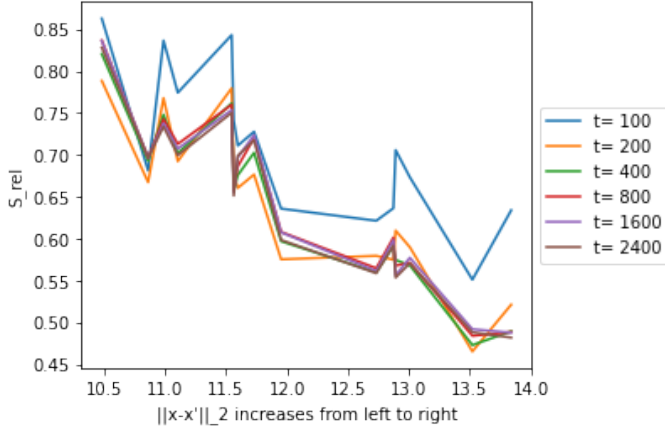


Fig. 3. $S_{\text{rel}}(t, \mathbf{x}', \mathbf{x})$ vs $\|\mathbf{x} - \mathbf{x}'\|_2$ (at a fixed \mathbf{x}'), at different times.

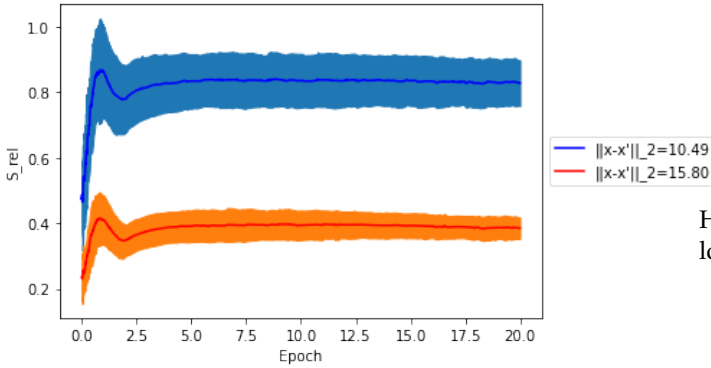


Fig. 4. S_{rel} 's time evolution at two pairs of points of $(\mathbf{x}, \mathbf{x}')$ at different mutual distances for a fixed \mathbf{x}' .

3 TRACKING S_{rel} FOR PENALIZED LINEAR REGRESSION OVER FEATURES AND CLASSIFICATION DATA

Penalized linear regression over features can always be imagined as training over the last layer of a neural net where the fixed features are the outputs of the last layer of activations on the training data. Thus motivated we define

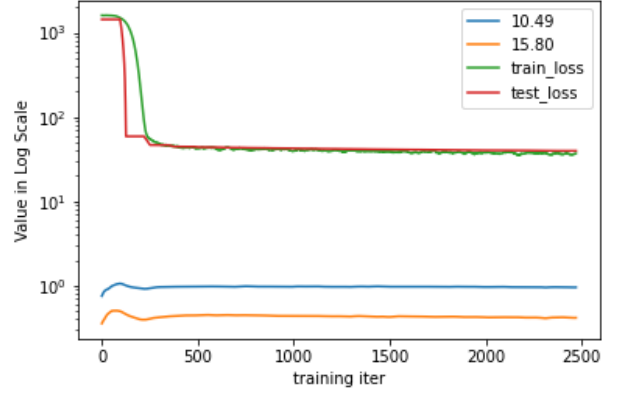


Fig. 5. In here we plot the mean values of the plots of Figure 4 overlaid against the time evolution of the mean values of the empirical and the population risks during the same experiment.

the following main quantities for the last layer of a neural net,

- Let the last layer be mapping, $\mathbb{R}^p \rightarrow \mathbb{R}^K$ with its weight matrix being $W \in \mathbb{R}^{K \times p}$ and its i^{th} -row being $\mathbf{w}_i \in \mathbb{R}^p$.
- Corresponding to K possible classes we consider the training data set to be of the form $(\mathbf{x}_i, \mathbf{y}_i)$ where for each $k \in \{1, \dots, K\}$, $n_k \in \mathbb{Z}^+$ of these tuples are s.t their $\mathbf{y}_i = \mathbf{e}_k \in \mathbb{R}^K$ (the k^{th} standard basis in \mathbb{R}^K). Hence we can define the total size of the training data as $\mathcal{N} := \sum_{k=1}^K n_k$
- We assume an arbitrary ordering among the n_k training data in the k^{th} -class. Thus $\mathbf{h}_{k,i} \in \mathbb{R}^p$ would be defined as the output of the gates at the last hidden layer when the input is the i^{th} -training data of the k^{th} -class.

Hence given a positive constant, λ_1 we define the following loss function for the last layer,

$$\mathcal{L}(W) = \frac{1}{2 \cdot \mathcal{N}} \sum_{k=1}^K \sum_{i=1}^{n_k} \|\mathbf{e}_k - W \mathbf{h}_{k,i}\|^2 + \frac{\lambda_1}{2K} \sum_{k=1}^K \|\mathbf{w}_k\|^2 \quad (3)$$

It is clear that the above loss function explicitly biases the optimization towards finding solutions where, $\frac{1}{2K} \sum_{k=1}^K \|\mathbf{w}_k\|^2$ is small. We can rewrite the above in terms of loss functions evaluated at each data point, $\mathcal{L}(W; \mathbf{h}_{k,i})$. Thus we have,

$$\begin{aligned}
\frac{\partial \mathcal{L}}{\partial \mathbf{w}_q} &= \frac{1}{\mathcal{N}} \cdot \sum_{k'=1}^K \sum_{i'=1}^{n_k} \frac{\partial \mathcal{L}(W; \mathbf{h}_{k',i'})}{\partial \mathbf{w}_q} \\
&= \frac{1}{\mathcal{N}} \cdot \sum_{k'=1}^K \sum_{i'=1}^{n_k} \left((\delta_{k',q} - \langle \mathbf{w}_q, \mathbf{h}_{k',i'} \rangle) (-\mathbf{h}_{k',i'}) + \frac{\mathcal{N}\lambda_1}{K} \mathbf{w}_q \right) \\
&= - \left(\frac{1}{\mathcal{N}} \sum_{k'=1}^K \sum_{i'=1}^{n_k} \delta_{k',q} \mathbf{h}_{k',i'} \right) \\
&\quad + \frac{\mathcal{N}\lambda_1}{K} \mathbf{w}_q + \left(\frac{1}{\mathcal{N}} \cdot \sum_{k',i'} \mathbf{h}_{k',i'} \mathbf{h}_{k',i'}^\top \right) \mathbf{w}_q
\end{aligned}$$

Now we can define constants, $\beta^2 := 1$, $\mathbf{u}_q := \frac{1}{\mathcal{N}} \cdot \sum_{i'=1}^{n_q} \mathbf{h}_{q,i'}$ and $\mathbb{R}^{p \times p} \ni \mathbf{M} := \frac{\mathcal{N}\lambda_1}{K} \mathbf{I}_p + \frac{1}{\mathcal{N}} \cdot \sum_{k',i'} \mathbf{h}_{k',i'} \mathbf{h}_{k',i'}^\top$.

Thus we can rewrite the above as, $\frac{\partial \mathcal{L}}{\partial \mathbf{w}_q} = -\beta^2 \mathbf{u}_q + \mathbf{M} \mathbf{w}_q$

Definition 4. Given a $\theta \in \mathbb{R}$, we define the gradient flow time evolution of the rows of the matrix W to be happening via the following O.D.E,

$$\frac{d\mathbf{w}_q}{dt} = -\theta^2 \cdot \frac{\partial \mathcal{L}}{\partial \mathbf{w}_q} = \theta^2 \beta^2 \mathbf{u}_q - \theta^2 \mathbf{M} \mathbf{w}_q$$

Theorem 3.1. Since \mathbf{M} is P.D (given $\lambda_1 > 0$), we can integrate the O.D.E in Definition 4, to get,

$$\mathbf{w}_q(t) = e^{-\theta^2 \mathbf{M} t} \left[\mathbf{w}_q(0) + \beta^2 \mathbf{M}^{-1} \mathbf{u}_q \right] - \beta^2 \mathbf{M}^{-1} \mathbf{u}_q$$

The proof of the above is immediate.

Theorem 3.2. We imagine the loss function in equation 3 to be over a linear predictor with weight matrix W whose rows are evolving as given in Theorem 3.1. Then invoking the definition of S_{rel} , as in Definition 1, for $\mathbf{x} = (k, i)^{\text{th}}$ -data point and $\mathbf{x}' = (c, j)^{\text{th}}$ -data point we get,

$$\begin{aligned}
S_{\text{rel}}^2(t)_{(c,j),(k,i)} &= \frac{\|W^+ \mathbf{h}_{c,j} - W \mathbf{h}_{k,i}\|^2}{\|W^+ \mathbf{h}_{k,i} - W \mathbf{h}_{c,j}\|^2} \\
&= \frac{\|\mathbf{h}_{c,j}^\top \cdot \mathbf{h}_{k,i}\|^2 - 2 \langle \mathbf{h}_{c,j}, \mathbf{h}_{k,i} \rangle \cdot \langle \mathbf{T}_{k,i} \mathbf{h}_{c,j}, \mathbf{w}_k \rangle + \sum_{q=1}^K \langle \mathbf{T}_{k,i} \mathbf{h}_{c,j}, \mathbf{w}_q \rangle^2}{\|\mathbf{h}_{k,i}\|^4 - 2 \tilde{h}_{k,i} \cdot \|\mathbf{h}_{k,i}\|^2 \cdot \langle \mathbf{h}_{k,i}, \mathbf{w}_k \rangle + \tilde{h}_{k,i}^2 \cdot \sum_{q=1}^K \langle \mathbf{h}_{k,i}, \mathbf{w}_q \rangle^2}
\end{aligned} \quad (4)$$

where we have defined $\tilde{h}_{k,i} := \left[\frac{\mathcal{N}\lambda_1}{K} + \|\mathbf{h}_{k,i}\|^2 \right]$ and the matrices, $\mathbb{R}^{p \times p} \ni \mathbf{T}_{k,i} := \frac{\mathcal{N}\lambda_1}{K} \mathbf{I}_p + \mathbf{h}_{k,i} \mathbf{h}_{k,i}^\top$

We note that the time dependence of the above expression is only via the $\{\mathbf{w}_i \in \mathbb{R}^p \mid i = 1, \dots, K\}$, the row vectors of W , which have been defined to be evolving as given in Theorem 3.1

In the following subsection we shall see an explicit instantiation of the above formula leading to a demonstration that non-trivial dynamics of S_{rel} is possible for even linear predictors when a regularization is used.

Proof of Theorem 3.2. We can read off, that corresponding to sampling the $(k, i)^{\text{th}}$ -data point and a choice of step-length η , for the q^{th} -row of W we would have,

$$\mathbf{w}_q^+ = \mathbf{w}_q - \eta \cdot \frac{\partial \mathcal{L}(W; \mathbf{h}_{k,i})}{\partial \mathbf{w}_q} = \mathbf{w}_q - \eta \cdot (-\delta_{k,q} \mathbf{h}_{k,i} + \mathbf{T}_{k,i} \mathbf{w}_q)$$

As a consequence of the fictitious update above the norm squared of the change in the output at the training data point (c, j) for some $c \in \{1, \dots, K\}$ and $j \in \{1, \dots, n_c\}$ is given as,

$$\begin{aligned}
&\|W^+ \mathbf{h}_{c,j} - W \mathbf{h}_{c,j}\|^2 \\
&= \sum_{q=1}^K \left(\langle \mathbf{w}_q^+, \mathbf{h}_{c,j} \rangle - \langle \mathbf{w}_q, \mathbf{h}_{c,j} \rangle \right)^2 \\
&= \eta^2 \cdot \sum_{q=1}^K \left(-\delta_{k,q} \mathbf{h}_{k,i} + \mathbf{T}_{k,i} \mathbf{w}_q, \mathbf{h}_{c,j} \right)^2 \\
&= \eta^2 \cdot \sum_{q=1}^K \left(-\delta_{k,q} \langle \mathbf{h}_{k,i}, \mathbf{h}_{c,j} \rangle + \mathbf{h}_{c,j}^\top \mathbf{T}_{k,i} \mathbf{w}_q \right)^2 \\
&= \eta^2 \cdot \sum_{q=1}^K \left\{ \delta_{k,q} \left(\langle \mathbf{h}_{k,i}, \mathbf{h}_{c,j} \rangle^2 - 2 \cdot \langle \mathbf{h}_{k,i}, \mathbf{h}_{c,j} \rangle \cdot \mathbf{h}_{c,j}^\top \mathbf{T}_{k,i} \mathbf{w}_q \right) \right\} \\
&\quad + \eta^2 \cdot \sum_{q=1}^K \left(\mathbf{h}_{c,j}^\top \mathbf{T}_{k,i} \mathbf{w}_q \right)^2 \\
&= \eta^2 \left(\langle \mathbf{h}_{k,i}, \mathbf{h}_{c,j} \rangle^2 - 2 \cdot \langle \mathbf{h}_{k,i}, \mathbf{h}_{c,j} \rangle \cdot \mathbf{h}_{c,j}^\top \mathbf{T}_{k,i} \mathbf{w}_k \right) \\
&\quad + \eta^2 \mathbf{h}_{c,j}^\top \mathbf{T}_{k,i} \left(\sum_{q=1}^K \mathbf{w}_q \mathbf{w}_q^\top \right) \mathbf{T}_{k,i} \mathbf{h}_{c,j} \\
&= \eta^2 \|\mathbf{h}_{c,j}^\top \cdot \mathbf{h}_{k,i}\|^2 - 2\eta^2 \langle \mathbf{h}_{k,i}, \mathbf{h}_{c,j} \rangle \cdot \langle \mathbf{T}_{k,i} \mathbf{h}_{c,j}, \mathbf{w}_k \rangle \\
&\quad + \eta^2 \sum_{q=1}^K \langle \mathbf{T}_{k,i} \mathbf{h}_{c,j}, \mathbf{w}_q \rangle^2
\end{aligned}$$

In the last line above we have recalled that $\mathbf{T}_{k,i}$ is a symmetric matrix. Noting that $\mathbf{T}_{k,i} \mathbf{h}_{k,i} = \left[\frac{\mathcal{N}\lambda_1}{K} + \|\mathbf{h}_{k,i}\|^2 \right] \mathbf{h}_{k,i}$, we can read off from the above the final expression given in the theorem statement. \square

3.1 Experimental Demonstration of Equation 4 on Random Neural Features

We choose to work with 2 classes and hence $K = 2$ (and $W \in \mathbb{R}^{2 \times p}$ in the experiments) and we will always have $n_k = 10^3$ feature vectors per class and in all our experiments we fix $\lambda_1 = 1, \theta = 0.001$. For an experimental demonstration of the non-trivial time dynamics of equation 4, we need to instantiate the $\{\mathbf{h}_{k,i} \in \mathbb{R}^p \mid k = 1, \dots, K \ \& \ i = 1, \dots, n_k\}$ feature vectors via a choice of model. We create the $\mathbf{h}_{k,i}$ s as the outputs of a one hidden layer neural net mapping, $f_{\text{NN}} : \mathbb{R}^{\text{dim}} \ni \mathbf{x} \mapsto \text{ReLU}(W_r \mathbf{x}) \in \mathbb{R}^p$ for some $\text{dim} \in \mathbb{Z}^+$ whose $W_r \in \mathbb{R}^{p \times \text{dim}}$ matrix is randomly sampled from a Gaussian distribution. The input \mathbf{x} s to the above net are sampled from either of the two distributions,

- An isotropic Gaussian distribution whose along each coordinate the mean is 1 and variance is 2. These data are labelled with $\mathbf{e}_1 = (1, 0)$
- An isotropic Gaussian distribution whose along each coordinate the mean is 9 and variance is 1. These data are labelled with $\mathbf{e}_2 = (0, 1)$

Further, in computing equation 4, we choose $\mathbf{h}_{k,i}$ and $\mathbf{h}_{c,j}$ as the outputs of the above random net f_{NN} for an arbitrary pair of data points generated as above with labels \mathbf{e}_1 and \mathbf{e}_2 respectively.

In Figures 6, 7 and 8 we see the time dynamics of S_{rel} as given in equation 4 for the above setup for different values of p and dim. The plots are averaged over multiple time evolutions starting from random initial values for the two rows of the W matrix in equation 4.

From the figures we confirm the following two salient points,

- Firstly, we note the emergence of the conjectured two phase behaviour of S_{rel} , that there is always an initial time interval and a semi-infinite late time phase s.t the value of S_{rel} in the later is always larger than in the former.
 - Alongside the evolution of S_{rel} in all these figures we have also shown the evolution of the empirical loss as given in equation 3 for the above setup and evaluated once every 100 iterations.
- Its clear from the figures that the initial phase when the empirical loss is falling rapidly is always the time when S_{rel} is rising rapidly. And in late times when the empirical loss has approximately stabilized, S_{rel} too has stabilized.

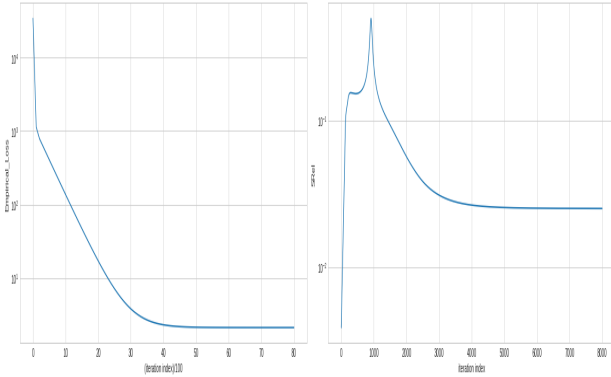


Fig. 6. $p = 10$, dim = 100

4 TRACKING S_{rel} FOR TRAINING A ReLU GATE BY AN ODE

In [33], the following algorithm was shown to train a ReLU gate (converge to a global minima of the risk) in linear time using very minimal distributional conditions if the labels are exactly realizable by a ground-truth weight \mathbf{w}_* of the ReLU gate.

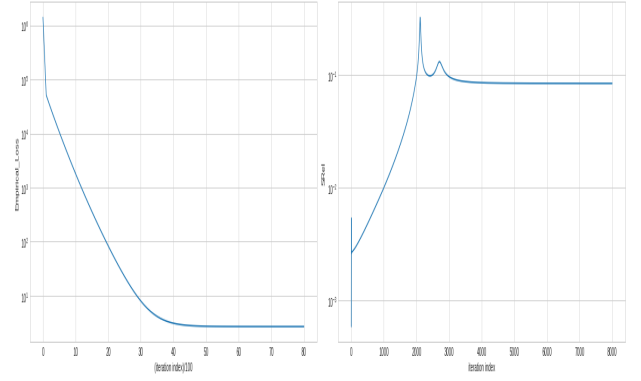


Fig. 7. $p = 50$, dim = 800

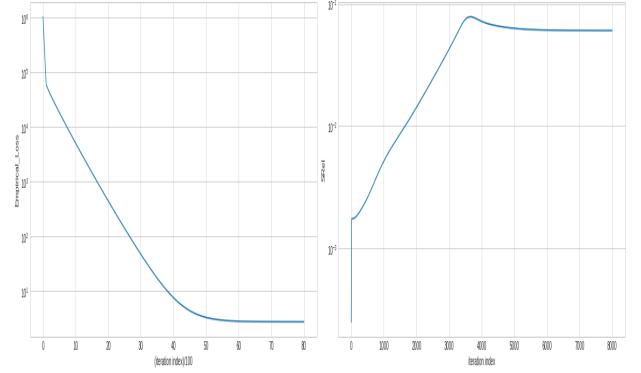


Fig. 8. $p = 400$, dim = 100

Algorithm 1 Modified S.G.D for training a ReLU gate in the realizable setting

- 1: **Input:** Sampling access to a distribution \mathcal{D} on \mathbb{R}^n .
- 2: **Input:** Oracle access to labels $\mathbb{R} \ni y = \text{ReLU}(\mathbf{w}_*^\top \mathbf{x})$ when queried with some $\mathbf{x} \in \mathbb{R}^n$
- 3: **Input:** An arbitrarily chosen starting point of $\mathbf{w}_1 \in \mathbb{R}^n$ and a step-length $\eta > 0$
- 4: **for** $t = 1, \dots$ **do**
- 5: Sample $\mathbf{x}_t \sim \mathcal{D}$ and query the oracle with it.
- 6: The oracle replies back with $y_t = \text{ReLU}(\mathbf{w}_*^\top \mathbf{x}_t)$
- 7: Form the gradient (proxy),

$$\mathbf{g}_t := -\mathbf{1}_{y_t > 0} (y_t - \mathbf{w}_t^\top \mathbf{x}_t) \mathbf{x}_t$$

- 8: $\mathbf{w}_{t+1} := \mathbf{w}_t - \eta \mathbf{g}_t$
- 9: **end for**

For some $\beta > 0$, a reasonable choice for the O.D.E. form of the algorithm 1 from [33] can be,

Definition 5.

$$\frac{d\mathbf{w}(t)}{dt} = \beta \cdot \mathbb{E}_{\mathbf{x} \sim \mathcal{D}} \left[\mathbf{1}_{\{\langle \mathbf{w}_*, \mathbf{x} \rangle > 0\}} \left(\max\{0, \langle \mathbf{w}_*, \mathbf{x} \rangle\} - \langle \mathbf{w}(t), \mathbf{x} \rangle \right) \mathbf{x} \right] \quad (5)$$

Theorem 4.1. If the matrix \mathbf{M} defined as $\mathbb{R}^{n \times n} \ni \mathbf{M} := \mathbb{E}[\mathbf{1}_{\{\mathbf{w}_*^\top \mathbf{x} > 0\}} \mathbf{x} \mathbf{x}^\top]$ is P.D, then for the ODE given in equation 5 we have, $\lim_{t \rightarrow \infty} \mathbf{w}(t) = \mathbf{w}_*$

Proof for Theorem 4.1. We define the following quantity towards writing the proof succinctly,

$$\mathbb{R}^n \ni \mathbf{z} := \mathbb{E} \left[\mathbb{1}_{\{\mathbf{w}_*^\top \mathbf{x} > 0\}} \max\{0, \mathbf{w}_*^\top \mathbf{x}\} \mathbf{x} \right] \quad (6)$$

Then the equation 5 can be written as,

$$\frac{d\mathbf{w}(t)}{dt} + \beta \mathbf{M} \mathbf{w} = \beta \mathbf{z} \implies \frac{d(e^{\beta \mathbf{M} t} \mathbf{w})}{dt} = e^{\beta \mathbf{M} t} \beta \mathbf{z} \quad (7)$$

The above can be integrated to get, $\mathbf{w}(t) = e^{-\beta \mathbf{M} t} \mathbf{w}(0) + \mathbf{M}^{-1} [\mathbf{I} - e^{-\beta \mathbf{M} t}] \mathbf{z}$

From the above solution it follows for the given assumptions about \mathbf{M} that, $\lim_{t \rightarrow \infty} \mathbf{w}(t) = \mathbf{M}^{-1} \mathbf{z}$. Now note that it follows from the definitions that $\mathbf{M} \mathbf{w}_* = \mathbf{z}$ and from the invertibility of \mathbf{M} the conclusion follows. \square

Now we can imagine the above ODE dynamics to be coming from a “risk function” (\mathcal{R}) and a loss function (ℓ) s.t we have,

$$\begin{aligned} \frac{d\mathbf{w}(t)}{dt} &= -\nabla_{\mathbf{w}} \mathcal{R} = \beta \{\mathbf{z} - \mathbf{M} \mathbf{w}\} \\ \nabla_{\mathbf{w}(t)} \ell(\mathbf{w}(t), \mathbf{x}) &= -\beta \mathbb{1}_{\{\mathbf{w}_*^\top \mathbf{x} > 0\}} [\max\{0, \mathbf{w}_*^\top \mathbf{x}\} - \mathbf{w}(t)^\top \mathbf{x}] \mathbf{x} \end{aligned} \quad (8)$$

The above motivates the following definition as needed for defining S_{rel} ,

$$\begin{aligned} \mathbf{w}^+(t) &= \mathbf{w}(t) - \eta \nabla_{\mathbf{w}(t)} \ell(\mathbf{w}(t), \mathbf{x}) \\ &= \mathbf{w}(t) + \eta \beta \mathbb{1}_{\{\mathbf{w}_*^\top \mathbf{x} > 0\}} [\max\{0, \mathbf{w}_*^\top \mathbf{x}\} - \mathbf{w}(t)^\top \mathbf{x}] \mathbf{x} \end{aligned} \quad (9)$$

Now we will observe the following two distinctive behaviours of the above quantity,

- In Lemma 4.2 we will see a simple *time independent* sufficient criteria to emerge for a candidate \mathbf{x}' i.e $\langle \mathbf{x}', \mathbf{x} \rangle$ being small, which would make the change in the prediction at \mathbf{x}' to be small because of this fictitious update of \mathbf{w}_t^+ based on a \mathbf{x} which makes an acute angle with \mathbf{w}_* .
- But in contrast at late times, we will show in Lemma 4.3 that S_{rel} cannot be arbitrarily small and we see that an easy sufficient condition emerges to ensure that S_{rel} is large i.e $|\langle \mathbf{x}', \mathbf{x} \rangle|$ being large for a fixed \mathbf{x} and for both the points making an acute angle with \mathbf{w}_* .

Lemma 4.2 (Proof in Appendix A.1).

$$\begin{aligned} &|\max\{0, \langle \mathbf{w}^+(t), \mathbf{x}' \rangle\} - \max\{0, \langle \mathbf{w}(t), \mathbf{x}' \rangle\}| \\ &\leq \eta \beta \mathbb{1}_{\{\langle \mathbf{w}_*, \mathbf{x} \rangle > 0\}} |\langle \mathbf{x}, \mathbf{x}' \rangle| \left| \left\langle e^{-\beta \mathbf{M} t} (\mathbf{w}(0) - \mathbf{w}_*), \mathbf{x} \right\rangle \right| \end{aligned}$$

Hence in words it follows that if $\langle \mathbf{w}_*, \mathbf{x} \rangle > 0$ then for all times, $|\langle \mathbf{x}, \mathbf{x}' \rangle|$ being small is sufficient condition for the change induced at \mathbf{x}' to be small when the update on $\mathbf{w}(t)$ is induced by sampling the data \mathbf{x} .

Theorem 4.3 (Proof in Appendix A.2). If $\langle \mathbf{w}_*, \mathbf{x}' \rangle > 0$ and $\langle \mathbf{w}_*, \mathbf{x} \rangle > 0$, then S_{rel} has the following lowerbound for late times,

$$\exists t_* \text{ s.t } \frac{|\langle \mathbf{x}, \mathbf{x}' \rangle|}{\|\mathbf{x}\|^2} \leq S_{\text{rel}}, \forall t > t_*$$

If we think of \mathbf{x}' and \mathbf{x} being in the same class given that they lie on the same side of the hyperplane defined by \mathbf{w}_* , it follows that later in the training $S_{\text{rel}}(\mathbf{x}, \mathbf{x}')$ can't be arbitrarily small for this ReLU training algorithm.

Further in support of the above model of training a ReLU gate and the above lowerbound on S_{rel} obtained therein we compare it to the dynamics of S_{rel} when using usual mini-batch S.G.D to minimize the standard ℓ_2 -risk on it in the realizable setting. In particular consider the risk corresponding to $\mathbf{w}_* = (1, 1, \dots, 1) \in \mathbb{R}^{10}$. In the following diagram, corresponding to $\mathbf{x} = (10, 10, \dots, 10)$ and $\mathbf{x}' = (\sqrt{200}, \sqrt{200}, \dots, \sqrt{200})$, we plot the dynamics of $S_{\text{rel}}(\mathbf{x}, \mathbf{x}')$ over iterations and averaged over multiple S.G.D runs - all of which converged to \mathbf{w}_* for all practical purposes.

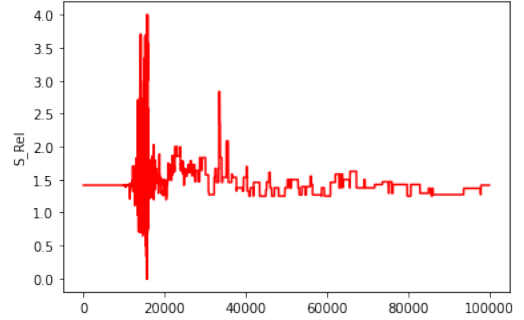


Fig. 9. Tracking S_{rel} (averaged over multiple runs of the algorithm) between a chosen pair of points for training a ReLU gate via mini-batch S.G.D in 10 dimensions in the realizable setting.

Note that for the above values of \mathbf{w}_* , \mathbf{x} and \mathbf{x}' , the late time lowerbound on S_{rel} given in Theorem 4.3 applies and it evaluates to ~ 1.4 which is very close to the value around which the above plot is fluctuating. Such experiments can be conducted under various other parameter settings lending further credence to this model. Thus here we again see that Conjecture 1.2 bears out.

Note that from combining equations 18 and 19 (in Appendix A.2) and their counterparts with \mathbf{x}' replaced with \mathbf{x} we can get an exact expression for S_{rel} for this situation of training a ReLU gate.

In the next section we shall move onto studying exactly provable behaviours of S_{rel} for certain polynomial hypothesis classes, which are strongly inspired from the study of large width neural nets.

5 TRACKING S_{rel} FOR GRADIENT FLOW ON ℓ_2 -LOSS ON DEGREE- d WEIGHT HOMOGENEOUS FEATURE LINEAR PREDICTORS

From ongoing theoretical research in algorithmic regularization and gradient dynamics on extremely wide neural

networks, [38], [39] certain kinds of high-degree polynomials have come to focus as being good test cases of various neural phenomenon. Inspired from these, we define the following class of functions which shall be the predictors we focus on in this segment,

Definition 6. For functions $\alpha : \mathbb{R}^n \rightarrow \mathbb{R}$ and $\beta_r : \mathbb{R}^n \rightarrow \mathbb{R}^n$, $r = 1, \dots, w$ we defined the “degree- d weight homogeneous feature linear predictors” as,

$$f_{d,w,\text{lin}}(W, \mathbf{x}) := \alpha(\mathbf{x}) + \sum_{r=1}^w \langle \beta_r(\mathbf{x}), \mathbf{w}_r^d \rangle$$

In above \mathbf{w}_r is used to denote the r^{th} -row of $W \in \mathbb{R}^{w \times n}$ and $\mathbf{w}_r^d := (w_{r,1}^d, \dots, w_{r,n}^d)$

Remark. As further motivation towards the above, we recall Theorem 2.1 in, [40]. In there it was assumed that each layer of the net say f_{NN} was of size $n = \dim(\mathbf{x})$ and hence each weight vector in each layer was of dimension n , which were in turn indexed as \mathbf{w}_r for $r = 1, \dots, w$. Then, given a point W_0 , (usually the value at initialization), the gradient dynamics on f_{NN} at asymptotically large widths was shown to be reproducible as gradient dynamics on a class of predictors which can be seen as a special case of Definition 6 corresponding to,

$$\begin{aligned} d &= 1 \\ \alpha(\mathbf{x}) &= f_{\text{NN}}(W_0, \mathbf{x}) - \langle \nabla_W f_{\text{NN}}(W, \mathbf{x}) |_{W=W_0}, W_0 \rangle \\ \beta_r(\mathbf{x}) &= \nabla_{\mathbf{w}_r} f_{\text{NN}}(W, \mathbf{x}) |_{W=W_0} \end{aligned}$$

The matrices W and W_0 when occurring inside the inner product are to be understood as having been vectorized row-wise.

We consider the ℓ_2 -loss evaluated on the above predictor for a data point (\mathbf{x}, y) ,

$$\begin{aligned} \ell_{d,w,\text{lin}}(W, (\mathbf{x}, y)) &:= \frac{1}{2} (y - f_{d,w,\text{lin}}(W, \mathbf{x}))^2 \\ &= \frac{1}{2} \left(y - \alpha(\mathbf{x}) - \sum_{r=1}^w \langle \beta_r(\mathbf{x}), \mathbf{w}_r^d \rangle \right)^2 \end{aligned} \quad (10)$$

If we denote W_t as the t^{th} iterate of a training algorithm on W with step-length η , then invoking Definition 1 in this context gives us,

$$\begin{aligned} [S_{\text{rel}}(t)]_{\mathbf{x}', \mathbf{x}} &:= \frac{|f_{d,w,\text{lin}}(W_t^+, \mathbf{x}') - f_{d,w,\text{lin}}(W_t, \mathbf{x}')|}{|f_{d,w,\text{lin}}(W_t^+, \mathbf{x}) - f_{d,w,\text{lin}}(W_t, \mathbf{x})|} \\ &\quad \text{where } \forall r \in \{1, \dots, w\} \\ \mathbf{w}_{r,t}^+ &= \mathbf{w}_{r,t} - \eta \nabla_{\mathbf{w}_r} \ell_{d,\text{lin}}(W_t, (\mathbf{x}, y)) \end{aligned} \quad (11)$$

Firstly, we demonstrate an time-independent upperbound for the above in the limit of small step-lengths,

Theorem 5.1 (A sufficient condition for the continuous time value of S_{rel} to be small, Proof in Appendix B.1).

$$\begin{aligned} &\lim_{\eta \rightarrow 0} [S_{\text{rel}}]_{\mathbf{x}', \mathbf{x}} \\ &\leq \left(\max_{r=1, \dots, w} \|\beta_r(\mathbf{x}') \odot \beta_r(\mathbf{x})\| \right) \cdot \sum_{r=1}^w \frac{\|\mathbf{w}_{r,t}^{2(d-1)}\|}{\left| \sum_{r=1}^w \langle \beta_r(\mathbf{x})^2, \mathbf{w}_{r,t}^{2(d-1)} \rangle \right|} \end{aligned}$$

Thus from above we can read off the “metric like” function induced on the data-space,

$$P(\mathbf{x}, \mathbf{x}') = \left(\max_{r=1, \dots, w} \|\beta_r(\mathbf{x}') \odot \beta_r(\mathbf{x})\| \right)$$

as envisaged in general in Conjecture 1.1.

5.1 Gradient flow dynamics for training $f_{d,w,\text{lin}}$

Now consider solving the learning problem $\min_{W \in \mathbb{R}^{w \times n}} \mathbb{E}_{(\mathbf{x}, y) \sim \mathcal{D}} [\ell_{d,w,\text{lin}}(W, (\mathbf{x}, y))]$ using the following gradient flow dynamics (which uses a parameter $\theta > 0$),

Definition 7 (Defining a gradient flow dynamics for training $f_{d,w,\text{lin}}$).

$$\begin{aligned} &\forall r \in \{1, \dots, w\} \\ &\frac{d\mathbf{w}_r(t)}{dt} \\ &= -\theta \frac{\partial}{\partial \mathbf{w}_r(t)} \mathbb{E}_{(\mathbf{x}, y) \sim \mathcal{D}} [\ell_{d,w,\text{lin}}(W, (\mathbf{x}, y))] \\ &= -\theta \frac{\partial}{\partial \mathbf{w}_r(t)} \mathbb{E}_{(\mathbf{x}, y)} \left[\frac{1}{2} \left(y - \alpha(\mathbf{x}) - \sum_{r=1}^w \langle \beta_r(\mathbf{x}), \mathbf{w}_r(t)^d \rangle \right)^2 \right] \\ &= \theta \cdot d \cdot \mathbb{E}_{(\mathbf{x}, y)} \left[\left(y - \alpha(\mathbf{x}) - \sum_{p=1}^w \langle \beta_p(\mathbf{x}), \mathbf{w}_p(t)^d \rangle \right) \cdot \left(\beta_r(\mathbf{x}) \odot \mathbf{w}_r(t)^{d-1} \right) \right] \end{aligned} \quad (12)$$

Theorem 5.2 (An exact expression for relative similarity for diagonal orthogonal quadratic features, Proof in Appendix B.2). Assume $w = n$ and suppose $\exists a_q \ \& \ b_q \ \forall q = 1, \dots, n$ s.t

$$\begin{aligned} a_q &:= \mathbb{E}_{(\mathbf{x}, y)} [(y - \alpha(\mathbf{x})) \beta_{q,q}(\mathbf{x})] \\ b_q \delta_{p,q} &:= \mathbb{E}_{(\mathbf{x}, y)} [\beta_{q,q}(\mathbf{x}) \beta_{p,p}(\mathbf{x})] \quad \forall p = 1, \dots, n \end{aligned}$$

Then for $d = 2$, $W = \text{diag}(\mathbf{w})$ for some $\mathbf{w} \in \mathbb{R}^n$, for features s.t $a_r > 0, \forall r \in \{1, \dots, n\}$ and initial conditions s.t $w_r(0)^2 \in (0, \frac{a_r}{b_r}) \ \forall r \in \{1, \dots, n\}$ for training via the ODE in equation 12, for S_{rel} , as defined via equations 10 and 11, we have,

$$\lim_{\eta \rightarrow 0} [S_{\text{rel}}]_{\mathbf{x}', \mathbf{x}} = \frac{\left| \sum_{r=1}^n \frac{a_r \beta_{r,r}(\mathbf{x}') \beta_{r,r}(\mathbf{x})}{b_r + \left\{ -b_r + \frac{a_r}{w_r^2(0)} \right\} e^{-4\theta a_r t}} \right|}{\left| \sum_{r=1}^n \frac{a_r \beta_{r,r}(\mathbf{x})^2}{b_r + \left\{ -b_r + \frac{a_r}{w_r^2(0)} \right\} e^{-4\theta a_r t}} \right|} \quad (13)$$

Remark. Note that the condition $a_r > 0, \forall r$ can be easily imagined to be satisfied if we have (A) “orthogonal features”

i.e $\forall p \neq q, 0 = \mathbb{E}_{(\mathbf{x}, y)} [\beta_{p,p}(\mathbf{x}) \cdot \beta_{q,q}(\mathbf{x})]$ (as already assumed in above) and (B) a “realizable” setting with $y = \alpha(\mathbf{x}) + \sum_{r=1}^w \theta_r^2 \beta_{r,r}(\mathbf{x})$ for some constants θ_r

For intuition, consider a special case of the above with $w = n = 3, \beta_{i,j}(\mathbf{z}) = z_i \delta_{i,j}, \forall i, j = \{1, 2, 3\}, \mathbf{z} \in \mathbb{R}^3, \mathbf{x} \sim \mathcal{N}(0, \mathbf{I}_{3 \times 3})$ and $y = \alpha(\mathbf{x}) + x_1 + 4x_2 + 9x_3$ for some $\alpha(\mathbf{x})$. Then $\forall i = 1, 2, 3, b_i = 1$. Then $\forall i = 1, 2, 3, a_i = \mathbb{E}_{\mathbf{x} \sim \mathcal{N}(0, \mathbf{I}_{3 \times 3})} [x_i \cdot (x_1 + 4x_2 + 9x_3)]$ which implies $a_1 = 1, a_2 = 4, a_3 = 9$. Then $\frac{b_1}{a_1} = 1, \frac{b_2}{a_2} = \frac{1}{4}, \frac{b_3}{a_3} = \frac{1}{9}$. And hence we can consistently choose $w_1(0)^2 = \frac{1}{2}, w_2(0)^2 = 2, w_3(0)^2 = 4$. Corresponding to the choices above, equation 13 reduces to, making the functional dependence on the parameters θ and t explicit,

$$\lim_{\eta \rightarrow 0} [S_{\text{rel}}](t)_{\theta, \mathbf{x}', \mathbf{x}} = \left| \frac{\frac{x'_1 x_1}{1 + e^{-4\theta t}} + \frac{x'_2 x_2}{\frac{1}{4} + \frac{1}{4} e^{-16\theta t}} + \frac{x'_3 x_3}{\frac{1}{9} + \frac{5}{36} e^{-36\theta t}}}{\frac{x_1^2}{1 + e^{-4\theta t}} + \frac{x_2^2}{\frac{1}{4} + \frac{1}{4} e^{-16\theta t}} + \frac{x_3^2}{\frac{1}{9} + \frac{5}{36} e^{-36\theta t}}} \right| \quad (14)$$

We will consider two ways of visualizing this formula,

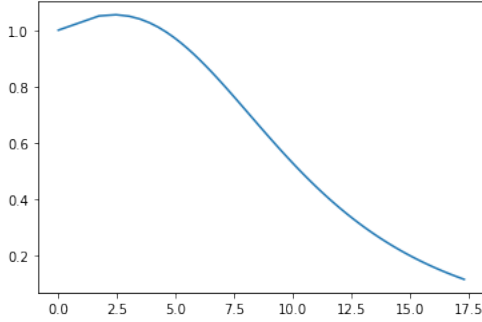
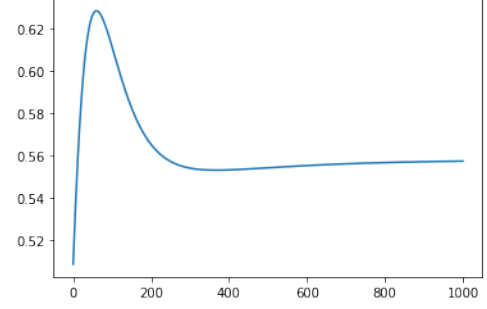


Fig. 10. In above we have chosen $\theta = 0.001, t = 500, \mathbf{x}' = (-1, -11, 1)$ and $\mathbf{x}(z) = \mathbf{x}' + (\sqrt{z}, \sqrt{z}, \sqrt{z})$ for $z = 1, 2, \dots, 100$ and then we have plotted S_{rel} (on the y -axis) as given in equation 14 as a function of $\|\mathbf{x}' - \mathbf{x}(z)\|$ (on the x -axis) which is increasing with z

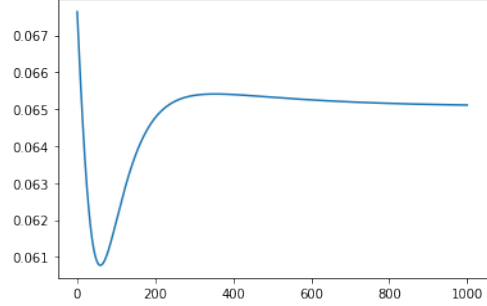
5.1.0.1 At all times S_{rel} decreases as \mathbf{x} gets farther away from \mathbf{x}' : The key property we observe in Figure 10 is that \exists a \hat{t} s.t $\forall t > \hat{t} S_{\text{rel}}(\mathbf{x}, \mathbf{x}')$ decreases as the sampled point \mathbf{x} is chosen farther away from the fixed testing point \mathbf{x}' . This property can be reproduced for various different paths of moving \mathbf{x} away from \mathbf{x}' . We observe the conceptual resemblance of the above figure with Figure 3 as were observed on neural nets.

5.1.0.2 For all $(\mathbf{x}, \mathbf{x}')$ S_{rel} is a non-decreasing function of time for all later times: In Figure 11 we plot equation 14 as a function of time for certain pairs of $(\mathbf{x}, \mathbf{x}')$. Note that the initial time behaviour S_{rel} is very different between Figures 11a and 11b but both of them demonstrate the validity of Conjecture 1.2 and values of t_1, t_2, t_* as in the conjecture can be read off from the plots.

More interestingly, now let us cast the setup of equation 14 as S.G.D solving the following class of risk minimization questions,



(a) In above we have chosen $\mathbf{x} = (1, -1, 1)$ and $\mathbf{x}' = (1.01, 0.999, 1.2)$.



(b) In above we have chosen $\mathbf{x} = (1, -11, 1)$ and $\mathbf{x}' = (1.01, 0.999, 1.2)$

Fig. 11. We plot the R.H.S of equation 14 for $t \in \{1, 2, \dots, 1000\}$ and $\theta = 0.001$

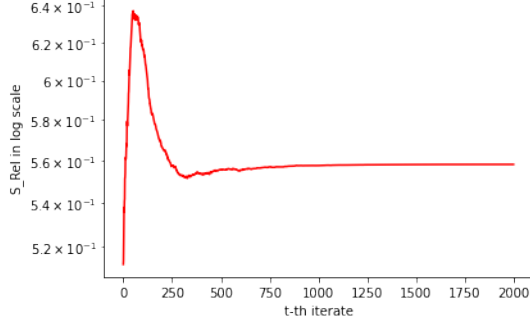
$$\begin{aligned} & \min_{\mathbf{w} \in \mathbb{R}^3} \mathbb{E}_{(\mathbf{x}, y)} [\ell(\mathbf{w}, (\mathbf{x}, y))] \\ & := \min_{\mathbf{w} \in \mathbb{R}^3} \mathbb{E}_{\mathbf{x} \sim \mathcal{N}(0, \mathbf{I}_{3 \times 3})} \left[\frac{1}{2} \left(y(\mathbf{x}) - \left(\alpha(\mathbf{x}) + \sum_{p=1}^3 \beta_{p,p}(\mathbf{x}) w_p^2 \right) \right)^2 \right] \end{aligned} \quad (15)$$

with $\beta_{p,p}(\mathbf{x}) = x_p$ for $p = 1, 2, 3$ as specified earlier and the true labels $y(\mathbf{x})$ being also generated as earlier $y(\mathbf{x}) = \alpha(\mathbf{x}) + \langle \mathbf{x}, \mathbf{w}_*^2 \rangle$ with $\mathbf{w}_* = (1, 2, 3)$. We denote $(w_{t,1}, w_{t,2}, w_{t,3}) = \mathbf{w}_t \in \mathbb{R}^3$ as the t^{th} -iterate of the S.G.D. We initialize the S.G.D at $w_{0,1} = \frac{1}{\sqrt{2}}, w_{0,2} = \sqrt{2}, w_{0,3} = 2$, the same initial conditions as used in deriving the O.D.E solution in equation 14 and use a step-length of $\eta = 0.001$ as was the value of the θ parameter in the plots in Figure 11. Then the t^{th} -step in the S.G.D would read,

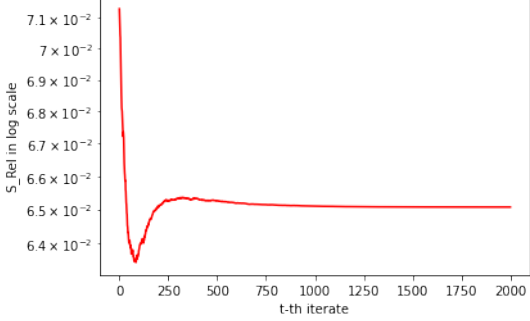
$$\begin{aligned} & \mathbf{x}_t \sim \mathcal{N}(0, \mathbf{I}_{3 \times 3}) \\ & \mathbf{w}_{t+1} = \mathbf{w}_t + 2\eta \left(\sum_{p=1}^3 x_{t,p} (\mathbf{w}_{*,p}^2 - \mathbf{w}_{t,p}^2) \right) \mathbf{x}_t \odot \mathbf{w}_t \end{aligned}$$

Thus at every \mathbf{w}_t for the above algorithm we can compute $S_{\text{rel}}(\mathbf{x}, \mathbf{x}')$ as given in Definition 1 with $\ell(\mathbf{w}_t, (\mathbf{x}, y))$ as given in Definition 15. In Figure 12 we give the corresponding plots averaged over many samples of S.G.D runs - and in all these samples the iterates were all eventually satisfying the condition $\|\mathbf{w}_t - \mathbf{w}_*\| < 10^{-6}$.

The sharp resemblance (of values as well as of the shape) between Figures 11 and 12, justifies our approach of modelling the behaviour of local elasticity for realistic training



(a) In above we have chosen $\mathbf{x} = (1, -1, 1)$ and $\mathbf{x}' = (1.01, 0.999, 1.2)$



(b) In above we have chosen $\mathbf{x} = (1, -11, 1)$ and $\mathbf{x}' = (1.01, 0.999, 1.2)$

Fig. 12. We plot S_{rel} for the t^{th} -iterate of S.G.D training on the risk given in equation 15 for $t \in \{1, 2, \dots, 2000\}$ and using step-length of $\eta = 0.001$. The plotted value is an average over multiple samples of S.G.D runs.

algorithms like S.G.D via appropriate limits of solutions of certain O.D.Es. For certain set of special cases of equation 13, in the next theorem we shall prove some of the key features observed in these two figures.

Theorem 5.3 (A special symmetric case with 2 features in 2 dimensions, Proof in Appendix B.3).

Suppose there are 2 features $\beta_1, \beta_2 : \mathbb{R}^2 \rightarrow \mathbb{R}^2$ and we are considering the following predictor class,

$$\mathbb{R}^2 \times \mathbb{R}^2 \ni (\mathbf{w}, \mathbf{x}) \mapsto f_{2,2,\text{lin}}(\mathbf{w}, \mathbf{x}) := \alpha(\mathbf{x}) + \sum_{r=1}^2 \beta_{r,r}(\mathbf{x}) \cdot w_r^2 \in \mathbb{R} \quad (16)$$

Now corresponding to a distribution over $\mathbb{R}^2 \times \mathbb{R}$, define $b_i := \mathbb{E}_{(\mathbf{x}, y)} [\beta_{i,i}(\mathbf{x})^2]$, $\forall i = 1, 2$ and $0 < a_i := \mathbb{E}_{(\mathbf{x}, y)} [(y - \alpha(\mathbf{x}))\beta_{i,i}(\mathbf{x})]$, $\forall i = 1, 2$

Suppose that $\exists \alpha, \beta \in \mathbb{R} \setminus \{0\}$ s.t,

$$\frac{b_1}{a_1} = \frac{b_2}{a_2} = \alpha^2$$

$$-\frac{b_1}{a_1} + \frac{1}{w_1(0)^2} = -\frac{b_2}{a_2} + \frac{1}{w_2(0)^2} = \beta^2$$

And we suppose the following condition on the features at the point \mathbf{x} and \mathbf{x}' being considered,

$$\frac{|\beta_{1,1}(\mathbf{x}')\beta_{1,1}(\mathbf{x}) + \beta_{2,2}(\mathbf{x}')\beta_{2,2}(\mathbf{x})|}{|\beta_{1,1}(\mathbf{x})^2 + \beta_{2,2}(\mathbf{x}')^2|} > 0$$

Then $\exists t^*$ s.t $\forall t \geq t^*$, $\lim_{\eta \rightarrow 0} [S_{\text{rel}}]_{\mathbf{x}', \mathbf{x}}$ (as defined via equations 10 and 11) is always bounded away from 0 and this lower bound is monotonically increasing with t .

We note that the above theorem is a partial evidence towards the property envisaged in Conjecture 1.2.

Remark. For intuition consider a special case of the above with $\beta_{i,i}(\mathbf{z}) = z_i$, $\forall i = \{1, 2\}$. Then we can write,

$$\frac{|\beta_{1,1}(\mathbf{x}')\beta_{1,1}(\mathbf{x}) + \beta_{2,2}(\mathbf{x}')\beta_{2,2}(\mathbf{x})|}{|\beta_{1,1}(\mathbf{x})^2 + \beta_{2,2}(\mathbf{x}')^2|} = \frac{|x'_1 x_1 + x'_2 x_2|}{|x_1^2 + x_2^2|} = \frac{|\langle \mathbf{x}', \mathbf{x} \rangle|}{\|\mathbf{x}\|^2}$$

Hence in this case the condition reduces to \mathbf{x}' not being orthogonal to \mathbf{x} for the S_{rel} to be prevented from being arbitrarily low.

6 CONCLUSION

In this work we were able to demonstrate via theory and neural experiments, a possibly general phenomenon that the weight updates in many popular training setups cause prediction changes preferably for only those data which are somehow “related” to the point being sampled for computing the stochastic gradient. And very crucially - and possibly surprisingly - our experiments in the classification setup showed that this preference sets in very early on in the training - much before the asymptotic classification accuracies have been attained. We recall that to pin down the above effect we had to introduce a new definition of “local elasticity” (Definition 3) which measures the changes in the predicted distribution over classes (for a fixed input) while the training is underway.

One of the main next steps from here on is to develop theoretical models where one can reproduce the phenomenon of local elasticity with neural classification experiments as demonstrated in Sections 2.1 and 2.2. More generally it would be an exciting avenue of future research to identify learning scenarios where the extended idea of S_{rel} as given in Definition 3 can be exactly calculated and thus its properties demonstrated in the experiments here being more firmly established as being characteristic of a large class of learning scenarios. Lastly, a necessary and sufficient condition on a learning process doing regression remains to be identified for which one can rigorously prove the late time non-decreasing behavior of S_{rel} .

ACKNOWLEDGMENTS

The authors would like to thank Prof. Weijie Su, Hangfeng He, Jiayao Zhang and Danny Wood for various discussions while writing this paper. Anirbit Mukherjee would like to thank Wharton Dean’s Fund for Postdoctoral Research and Prof. Weijie Su’s NSF CAREER DMS-1847415 for funding this research.

REFERENCES

- [1] D. Silver, A. Huang, C. J. Maddison, A. Guez, L. Sifre, G. Van Den Driessche, J. Schrittwieser, I. Antonoglou, V. Panneershelvam, M. Lanctot, *et al.*, “Mastering the game of go with deep neural networks and tree search,” *nature*, vol. 529, no. 7587, pp. 484–489, 2016.
- [2] D. Silver, J. Schrittwieser, K. Simonyan, I. Antonoglou, A. Huang, A. Guez, T. Hubert, L. Baker, M. Lai, A. Bolton, *et al.*, “Mastering the game of go without human knowledge,” *Nature*, vol. 550, no. 7676, pp. 354–359, 2017.
- [3] D. Silver, T. Hubert, J. Schrittwieser, I. Antonoglou, M. Lai, A. Guez, M. Lanctot, L. Sifre, D. Kumaran, T. Graepel, *et al.*, “A general reinforcement learning algorithm that masters chess, shogi, and go through self-play,” *Science*, vol. 362, no. 6419, pp. 1140–1144, 2018.
- [4] J. Schrittwieser, I. Antonoglou, T. Hubert, K. Simonyan, L. Sifre, S. Schmitt, A. Guez, E. Lockhart, D. Hassabis, T. Graepel, *et al.*, “Mastering atari, go, chess and shogi by planning with a learned model,” *Nature*, vol. 588, no. 7839, pp. 604–609, 2020.
- [5] M. H. Segler, M. Preuss, and M. P. Waller, “Planning chemical syntheses with deep neural networks and symbolic ai,” *Nature*, vol. 555, no. 7698, pp. 604–610, 2018.
- [6] H. Chen, O. Engkvist, Y. Wang, M. Olivecrona, and T. Blaschke, “The rise of deep learning in drug discovery,” *Drug discovery today*, vol. 23, no. 6, pp. 1241–1250, 2018.
- [7] M. Dalgaard, F. Motzoi, J. J. Sørensen, and J. Sherson, “Global optimization of quantum dynamics with alphazero deep exploration,” *npj Quantum Information*, vol. 6, no. 1, pp. 1–9, 2020.
- [8] T. Poggio, H. Mhaskar, L. Rosasco, B. Miranda, and Q. Liao, “Why and when can deep-but not shallow-networks avoid the curse of dimensionality: A review,” *International Journal of Automation and Computing*, pp. 1–17, 2017.
- [9] T. Poggio and Q. Liao, “Theory ii: Landscape of the empirical risk in deep learning,” *arXiv preprint arXiv:1703.09833*, 2017.
- [10] C. Zhang, Q. Liao, A. Rakhlin, K. Sridharan, B. Miranda, N. Golowich, and T. Poggio, “Theory of deep learning iii: Generalization properties of sgd,” tech. rep., Center for Brains, Minds and Machines (CBMM), 2017.
- [11] J. Lee, Y. Bahri, R. Novak, S. S. Schoenholz, J. Pennington, and J. Sohl-Dickstein, “Deep neural networks as gaussian processes,” 2017.
- [12] X. Wu, S. S. Du, and R. Ward, “Global convergence of adaptive gradient methods for an over-parameterized neural network,” *arXiv preprint arXiv:1902.07111*, 2019.
- [13] S. S. Du, J. D. Lee, H. Li, L. Wang, and X. Zhai, “Gradient descent finds global minima of deep neural networks,” 2018.
- [14] L. Su and P. Yang, “On learning over-parameterized neural networks: A functional approximation perspective,” in *Advances in Neural Information Processing Systems*, pp. 2637–2646, 2019.
- [15] K. Kawaguchi and J. Huang, “Gradient descent finds global minima for generalizable deep neural networks of practical sizes,” in *2019 57th Annual Allerton Conference on Communication, Control, and Computing (Allerton)*, pp. 92–99, IEEE, 2019.
- [16] J. Huang and H.-T. Yau, “Dynamics of deep neural networks and neural tangent hierarchy,” *arXiv preprint arXiv:1909.08156*, 2019.
- [17] Z. Allen-Zhu, Y. Li, and Z. Song, “A convergence theory for deep learning via over-parameterization,” in *International Conference on Machine Learning*, pp. 242–252, 2019.
- [18] Z. Allen-Zhu, Y. Li, and Y. Liang, “Learning and generalization in overparameterized neural networks, going beyond two layers,” in *Advances in neural information processing systems*, pp. 6155–6166, 2019.
- [19] Z. Allen-Zhu, Y. Li, and Z. Song, “On the convergence rate of training recurrent neural networks,” in *Advances in Neural Information Processing Systems*, pp. 6673–6685, 2019.
- [20] S. Du and J. Lee, “On the power of over-parametrization in neural networks with quadratic activation,” in *International Conference on Machine Learning*, pp. 1329–1338, 2018.
- [21] D. Zou, Y. Cao, D. Zhou, and Q. Gu, “Stochastic gradient descent optimizes over-parameterized deep relu networks,” *arXiv preprint arXiv:1811.08888*, 2018.
- [22] D. Zou and Q. Gu, “An improved analysis of training over-parameterized deep neural networks,” in *Advances in Neural Information Processing Systems*, pp. 2053–2062, 2019.
- [23] S. Arora, S. S. Du, W. Hu, Z. Li, R. R. Salakhutdinov, and R. Wang, “On exact computation with an infinitely wide neural net,” in *Advances in Neural Information Processing Systems*, pp. 8139–8148, 2019.
- [24] Z. Li, R. Wang, D. Yu, S. S. Du, W. Hu, R. Salakhutdinov, and S. Arora, “Enhanced convolutional neural tangent kernels,” *arXiv preprint arXiv:1911.00809*, 2019.
- [25] S. Arora, S. Du, W. Hu, Z. Li, and R. Wang, “Fine-grained analysis of optimization and generalization for overparameterized two-layer neural networks,” in *International Conference on Machine Learning*, pp. 322–332, 2019.
- [26] Z. Allen-Zhu and Y. Li, “What can resnet learn efficiently, going beyond kernels?,” in *Advances in Neural Information Processing Systems*, pp. 9015–9025, 2019.
- [27] C. Wei, J. D. Lee, Q. Liu, and T. Ma, “Regularization matters: Generalization and optimization of neural nets vs their induced kernel,” in *Advances in Neural Information Processing Systems*, pp. 9709–9721, 2019.
- [28] S. Goel, A. Klivans, and R. Meka, “Learning one convolutional layer with overlapping patches,” *arXiv preprint arXiv:1802.02547*, 2018.
- [29] S. Frei, Y. Cao, and Q. Gu, “Agnostic learning of a single neuron with gradient descent,” *arXiv preprint arXiv:2005.14426*, 2020.
- [30] S. Goel, S. Karmalkar, and A. Klivans, “Time/accuracy tradeoffs for learning a relu with respect to gaussian marginals,” in *Advances in Neural Information Processing Systems*, pp. 8584–8593, 2019.
- [31] I. Diakonikolas, S. Goel, S. Karmalkar, A. R. Klivans, and M. Soltanolkotabi, “Approximation schemes for relu regression,” in *Conference on Learning Theory*, 2020.
- [32] A. Mukherjee and R. Muthukumar, “Guarantees on learning depth-2 neural networks under a data-poisoning attack,” *arXiv preprint arXiv:2005.01699*, 2020.
- [33] A. Mukherjee and R. Muthukumar, “A study of neural training with non-gradient and noise assisted gradient methods,” *arXiv preprint arXiv:2005.04211*, 2020.
- [34] H. He and W. Su, “The local elasticity of neural networks,” in *International Conference on Learning Representations*, 2019.
- [35] S. Chen, H. He, and W. Su, “Label-aware neural tangent kernel: Toward better generalization and local elasticity,” *Advances in Neural Information Processing Systems*, vol. 33, 2020.
- [36] Y. Netzer, T. Wang, A. Coates, A. Bissacco, B. Wu, and A. Y. Ng, “Reading digits in natural images with unsupervised feature learning,” 2011.
- [37] A. Krizhevsky, G. Hinton, *et al.*, “Learning multiple layers of features from tiny images,” 2009.
- [38] Y. Bai and J. D. Lee, “Beyond linearization: On quadratic and higher-order approximation of wide neural networks,” in *International Conference on Learning Representations*, 2019.
- [39] B. Woodworth, S. Gunasekar, J. D. Lee, E. Moroshko, P. Savarese, I. Golan, D. Soudry, and N. Srebro, “Kernel and rich regimes in overparametrized models,” in *Conference on Learning Theory*, pp. 3635–3673, PMLR, 2020.
- [40] J. Lee, L. Xiao, S. Schoenholz, Y. Bahri, R. Novak, J. Sohl-Dickstein, and J. Pennington, “Wide neural networks of any depth evolve as linear models under gradient descent,” *Advances in neural information processing systems*, vol. 32, pp. 8572–8583, 2019.

APPENDIX A

PROOFS OF SECTION 4

A.1 Proof of Lemma 4.2

Proof.

$$\begin{aligned}
& \left| \max\{0, \langle \mathbf{w}^+(t), \mathbf{x}' \rangle\} - \max\{0, \langle \mathbf{w}(t), \mathbf{x}' \rangle\} \right| \\
&= \left| \max\{0, \langle \mathbf{w}(t), \mathbf{x} \rangle + \eta\beta \mathbb{1}_{\{\mathbf{w}_*^\top \mathbf{x} > 0\}} [\max\{0, \mathbf{w}_*^\top \mathbf{x}\} - \mathbf{w}(t)^\top \mathbf{x}] \langle \mathbf{x}, \mathbf{x}' \rangle \right. \\
&\quad \left. - \max\{0, \langle \mathbf{w}(t), \mathbf{x}' \rangle\} \right| \\
&\leq \eta\beta \mathbb{1}_{\{\langle \mathbf{w}_*, \mathbf{x} \rangle > 0\}} \left| \langle \mathbf{x}, \mathbf{x}' \rangle \right| \left| \max\{0, \mathbf{w}_*^\top \mathbf{x}\} - \mathbf{w}(t)^\top \mathbf{x} \right| \\
&\leq \eta\beta \mathbb{1}_{\{\langle \mathbf{w}_*, \mathbf{x} \rangle > 0\}} \left| \langle \mathbf{x}, \mathbf{x}' \rangle \right| \cdot \\
&\quad \left| \max\{0, \mathbf{w}_*^\top \mathbf{x}\} - \left\langle e^{-\beta \mathbf{M}t} \mathbf{w}(0), \mathbf{x} \right\rangle - \langle \mathbf{w}_*, \mathbf{x} \rangle + \left\langle e^{-\beta \mathbf{M}t} \mathbf{w}_*, \mathbf{x} \right\rangle \right| \\
&\leq \eta\beta \mathbb{1}_{\{\langle \mathbf{w}_*, \mathbf{x} \rangle > 0\}} \left| \langle \mathbf{x}, \mathbf{x}' \rangle \right| \left| \left\langle e^{-\beta \mathbf{M}t} (\mathbf{w}(0) - \mathbf{w}_*), \mathbf{x} \right\rangle \right|
\end{aligned} \tag{17}$$

□

A.2 Proof of Theorem 4.3

Proof. Starting similarly as in the above proof we see that,

$$\begin{aligned}
\langle \mathbf{w}^+(t), \mathbf{x}' \rangle &= \langle \mathbf{w}(t), \mathbf{x}' \rangle + \eta\beta \mathbb{1}_{\{\mathbf{w}_*^\top \mathbf{x} > 0\}} [\mathbf{w}_* - \mathbf{w}(t)]^\top \mathbf{x} \cdot \langle \mathbf{x}, \mathbf{x}' \rangle \\
&= \langle \mathbf{w}(t), \mathbf{x}' \rangle + \eta\beta \mathbb{1}_{\{\mathbf{w}_*^\top \mathbf{x} > 0\}} \left[e^{-\beta \mathbf{M}t} (\mathbf{w}_* - \mathbf{w}(0)) \right]^\top \mathbf{x} \cdot \langle \mathbf{x}, \mathbf{x}' \rangle \\
&= \langle \mathbf{w}_*, \mathbf{x}' \rangle + \left\langle e^{-\beta \mathbf{M}t} (\mathbf{w}(0) - \mathbf{w}_*), \mathbf{x}' \right\rangle \\
&\quad + \eta\beta \mathbb{1}_{\{\mathbf{w}_*^\top \mathbf{x} > 0\}} \left[e^{-\beta \mathbf{M}t} (\mathbf{w}_* - \mathbf{w}(0)) \right]^\top \mathbf{x} \cdot \langle \mathbf{x}, \mathbf{x}' \rangle
\end{aligned} \tag{18}$$

Further let us define α_1 & α_2 as,

$$\begin{aligned}
\alpha_1 &:= \langle \mathbf{w}(t), \mathbf{x}' \rangle - \left\langle e^{-\beta \mathbf{M}t} (\mathbf{w}(0) - \mathbf{w}_*), \mathbf{x}' \right\rangle + \langle \mathbf{w}_*, \mathbf{x}' \rangle \\
\alpha_2 &:= \eta\beta \mathbb{1}_{\{\mathbf{w}_*^\top \mathbf{x} > 0\}} \left[e^{-\beta \mathbf{M}t} (\mathbf{w}_* - \mathbf{w}(0)) \right]^\top \mathbf{x} \cdot \langle \mathbf{x}, \mathbf{x}' \rangle
\end{aligned} \tag{19}$$

Hence we have, $|\max\{0, \langle \mathbf{w}(t)^+, \mathbf{x}' \rangle\} - \max\{0, \langle \mathbf{w}(t), \mathbf{x}' \rangle\}| = |\max\{0, \alpha_1 + \alpha_2\} - \max\{0, \alpha_1\}|$

Now we invoke the assumption that $\langle \mathbf{w}_*, \mathbf{x}' \rangle > 0$ and the fact that anything weighted by $e^{-\beta \mathbf{M}t}$ is monotonically decreasing in time to 0 in absolute value to realize that $\exists t_* > 0$ s.t $\forall t > t_*$ we have $\alpha_1 > 0$ & $\alpha_1 + \alpha_2 > 0$. Hence,

$$\begin{aligned}
\forall t > t_*, |\max\{0, \langle \mathbf{w}(t)^+, \mathbf{x}' \rangle\} - \max\{0, \langle \mathbf{w}(t), \mathbf{x}' \rangle\}| \\
&= |\alpha_2| = \eta\beta \left| \left\langle e^{-\beta \mathbf{M}t} (\mathbf{w}_* - \mathbf{w}(0)), \mathbf{x} \right\rangle \right| \left| \langle \mathbf{x}, \mathbf{x}' \rangle \right|
\end{aligned} \tag{20}$$

We further invoke Lemma 4.2 to get,

$$\left| \max\{0, \langle \mathbf{w}(t)^+, \mathbf{x} \rangle\} - \max\{0, \langle \mathbf{w}(t), \mathbf{x} \rangle\} \right| \leq \eta\beta \mathbb{1}_{\{\langle \mathbf{w}_*, \mathbf{x} \rangle > 0\}} \|\mathbf{x}\|^2 \left| \left\langle e^{-\beta \mathbf{M}t} (\mathbf{w}(0) - \mathbf{w}_*), \mathbf{x} \right\rangle \right|$$

Combining this with equation 20 we get the following lowerbound for S_{rel} ,

$$\frac{\eta\beta \left| \left\langle e^{-\beta \mathbf{M}t} (\mathbf{w}_* - \mathbf{w}(0)), \mathbf{x} \right\rangle \right| \left| \langle \mathbf{x}, \mathbf{x}' \rangle \right|}{\eta\beta \mathbb{1}_{\{\langle \mathbf{w}_*, \mathbf{x} \rangle > 0\}} \|\mathbf{x}\|^2 \left| \left\langle e^{-\beta \mathbf{M}t} (\mathbf{w}(0) - \mathbf{w}_*), \mathbf{x} \right\rangle \right|} \leq S_{\text{rel}}, \forall t > t_* \tag{21}$$

Invoking the assumption that $\langle \mathbf{w}_*, \mathbf{x} \rangle > 0$ we can write the more succinct lowerbound as stated in the lemma,

$$\frac{|\langle \mathbf{x}, \mathbf{x}' \rangle|}{\|\mathbf{x}\|^2} \leq S_{\text{rel}}, \forall t > t_*, \tag{22}$$

□

APPENDIX B

PROOFS OF SECTION 5

B.1 Proof of Theorem 5.1

Proof. Simplifying equations 10 and 11 we get,

$$\begin{aligned} \mathbf{w}_{r,t}^+ - \mathbf{w}_{r,t} &= -\eta \nabla_{\mathbf{w}_{r,t}} \ell_{d,w,\text{lin}}(W_t, (\mathbf{x}, y)) \\ &= \eta \left(y - \alpha(\mathbf{x}) - \sum_{p=1}^w \langle \beta_p(\mathbf{x}), \mathbf{w}_{p,t}^d \rangle \right) \cdot d \cdot (\beta_r(\mathbf{x}) \odot \mathbf{w}_{r,t}^{d-1}) \end{aligned} \quad (23)$$

Hence,

$$\begin{aligned} &\mathbf{w}_{r,t}^{+d} - \mathbf{w}_{r,t}^d \\ &= \left(\mathbf{w}_{r,t} + \eta \left(y - \alpha(\mathbf{x}) - \sum_{p=1}^w \langle \beta_p(\mathbf{x}), \mathbf{w}_{p,t}^d \rangle \right) \cdot d \cdot (\beta_r(\mathbf{x}) \odot \mathbf{w}_{r,t}^{d-1}) \right)^d - \mathbf{w}_{r,t}^d \\ &= \sum_{k=1}^d \binom{d}{k} (\eta \cdot d)^k \cdot \left(y - \alpha(\mathbf{x}) - \sum_{p=1}^w \langle \beta_p(\mathbf{x}), \mathbf{w}_{p,t}^d \rangle \right)^k \cdot \mathbf{w}_{r,t}^{d-k} \odot (\beta_r(\mathbf{x}) \odot \mathbf{w}_{r,t}^{d-1})^k \end{aligned} \quad (24)$$

From the Definition 6 it follows that,

$$\begin{aligned} &f_{d,w,\text{lin}}(W_t^+, \mathbf{x}') - f_{d,w,\text{lin}}(W_t, \mathbf{x}') \\ &= \sum_{r=1}^w \langle \beta_r(\mathbf{x}'), \mathbf{w}_{r,t}^{+d} - \mathbf{w}_{r,t}^d \rangle \\ &= \sum_{r=1}^w \sum_{k=1}^d \binom{d}{k} (\eta \cdot d)^k \cdot \left(y - \alpha(\mathbf{x}) - \sum_{p=1}^w \langle \beta_p(\mathbf{x}), \mathbf{w}_{p,t}^d \rangle \right)^k \cdot \langle \beta_r(\mathbf{x}') \odot \beta_r(\mathbf{x})^k, \mathbf{w}_{r,t}^{d(k+1)-2k} \rangle \end{aligned} \quad (25)$$

In the second equality above we have used the following fact,

$$\begin{aligned} \langle \beta_r(\mathbf{x}'), \mathbf{w}_{r,t}^{d-k} \odot (\beta_r(\mathbf{x}) \odot \mathbf{w}_{r,t}^{d-1})^k \rangle &= \sum_{i=1}^n \beta_{r,i}(\mathbf{x}') \cdot \mathbf{w}_{r,t,i}^{d-k} \cdot \beta_{r,i}(\mathbf{x})^k \cdot \mathbf{w}_{r,t,i}^{k(d-1)} \\ &= \langle \beta_r(\mathbf{x}') \odot \beta_r(\mathbf{x})^k, \mathbf{w}_{r,t}^{d(k+1)-2k} \rangle \end{aligned} \quad (26)$$

Similar to the above we can read off,

$$\begin{aligned} &f_{d,w,\text{lin}}(W_t^+, \mathbf{x}) - f_{d,w,\text{lin}}(W_t, \mathbf{x}) \\ &= \sum_{r=1}^w \sum_{k=1}^d \binom{d}{k} (\eta \cdot d)^k \cdot \left(y - \alpha(\mathbf{x}) - \sum_{p=1}^w \langle \beta_p(\mathbf{x}), \mathbf{w}_{p,t}^d \rangle \right)^k \cdot \langle \beta_r(\mathbf{x})^{k+1}, \mathbf{w}_{r,t}^{d(k+1)-2k} \rangle \end{aligned} \quad (27)$$

B.1.0.1 The limit of $\eta \rightarrow 0$: Now we note that,

$$\begin{aligned} &\lim_{\eta \rightarrow 0} \frac{1}{\eta} \cdot |f_{d,w,\text{lin}}(W_t^+, \mathbf{x}') - f_{d,w,\text{lin}}(W_t, \mathbf{x}')| \\ &= \left| \sum_{r=1}^w d^2 \cdot \left(y - \alpha(\mathbf{x}) - \sum_{p=1}^w \langle \beta_p(\mathbf{x}), \mathbf{w}_{p,t}^d \rangle \right) \cdot \langle \beta_r(\mathbf{x}') \odot \beta_r(\mathbf{x}), \mathbf{w}_{r,t}^{2(d-1)} \rangle \right| \end{aligned} \quad (28)$$

And similarly,

$$\begin{aligned} &\lim_{\eta \rightarrow 0} \frac{1}{\eta} \cdot |f_{d,w,\text{lin}}(W_t^+, \mathbf{x}) - f_{d,w,\text{lin}}(W_t, \mathbf{x})| \\ &= \left| \sum_{r=1}^w d^2 \cdot \left(y - \alpha(\mathbf{x}) - \sum_{p=1}^w \langle \beta_p(\mathbf{x}), \mathbf{w}_{p,t}^d \rangle \right) \cdot \langle \beta_r(\mathbf{x})^2, \mathbf{w}_{r,t}^{2(d-1)} \rangle \right| \end{aligned} \quad (29)$$

If S_{rel} is well defined then we can write,

$$\begin{aligned}
\lim_{\eta \rightarrow 0} [S_{\text{rel}}]_{\mathbf{x}', \mathbf{x}} &= \lim_{\eta \rightarrow 0} \frac{\frac{1}{\eta} \cdot |f_{\text{d,w,lin}}(\mathbf{W}_t^+, \mathbf{x}') - f_{\text{d,w,lin}}(\mathbf{W}_t, \mathbf{x}')|}{\frac{1}{\eta} \cdot |f_{\text{d,w,lin}}(\mathbf{W}_t^+, \mathbf{x}) - f_{\text{d,w,lin}}(\mathbf{W}_t, \mathbf{x})|} \\
&= \frac{\left| \sum_{r=1}^w d^2 \cdot (y - \alpha(\mathbf{x}) - \sum_{p=1}^w \langle \beta_p(\mathbf{x}), \mathbf{w}_{p,t}^d \rangle) \cdot \langle \beta_r(\mathbf{x}') \odot \beta_r(\mathbf{x}), \mathbf{w}_{r,t}^{2(d-1)} \rangle \right|}{\left| \sum_{r=1}^w d^2 \cdot (y - \alpha(\mathbf{x}) - \sum_{p=1}^w \langle \beta_p(\mathbf{x}), \mathbf{w}_{p,t}^d \rangle) \cdot \langle \beta_r(\mathbf{x}) \odot \beta_r(\mathbf{x}), \mathbf{w}_{r,t}^{2(d-1)} \rangle \right|} \\
&= \frac{\left| \sum_{r=1}^w \langle \beta_r(\mathbf{x}') \odot \beta_r(\mathbf{x}), \mathbf{w}_{r,t}^{2(d-1)} \rangle \right|}{\left| \sum_{r=1}^w \langle \beta_r(\mathbf{x})^2, \mathbf{w}_{r,t}^{2(d-1)} \rangle \right|}
\end{aligned} \tag{30}$$

Hence from equation 30 we have the expression that we set out to prove,

$$\begin{aligned}
\lim_{\eta \rightarrow 0} [S_{\text{rel}}]_{\mathbf{x}', \mathbf{x}} &\leq \sum_{r=1}^w \|\beta_r(\mathbf{x}') \odot \beta_r(\mathbf{x})\| \cdot \frac{\|\mathbf{w}_{r,t}^{2(d-1)}\|}{\left| \sum_{r=1}^w \langle \beta_r(\mathbf{x})^2, \mathbf{w}_{r,t}^{2(d-1)} \rangle \right|} \\
\implies \lim_{\eta \rightarrow 0} [S_{\text{rel}}]_{\mathbf{x}', \mathbf{x}} &\leq \left(\max_{r=1, \dots, w} \|\beta_r(\mathbf{x}') \odot \beta_r(\mathbf{x})\| \right) \cdot \sum_{r=1}^w \frac{\|\mathbf{w}_{r,t}^{2(d-1)}\|}{\left| \sum_{r=1}^w \langle \beta_r(\mathbf{x})^2, \mathbf{w}_{r,t}^{2(d-1)} \rangle \right|}
\end{aligned} \tag{31}$$

□

B.2 Proof of Theorem 5.2

Proof. Upon invoking the assumptions $w = n$ & $\mathbf{W} = \text{diag}(\mathbf{w})$ for some $\mathbf{w} \in \mathbb{R}^n$ and denoting the q^{th} coordinate of \mathbf{w} to be w_q , equation 12 will reduce to,

$$\begin{aligned}
&\forall q \in \{1, \dots, n\} \\
\frac{1}{\theta d} \cdot \frac{dw_q(t)}{dt} &= \mathbb{E}_{(\mathbf{x}, y)} \left[\left(y - \alpha(\mathbf{x}) - \sum_{p=1}^n \beta_{p,p}(\mathbf{x}) \cdot w_p(t)^d \right) \cdot (\beta_{q,q}(\mathbf{x}) \cdot w_q(t)^{d-1}) \right]
\end{aligned} \tag{32}$$

We recall the definition of a_q and we define a new set of distribution dependent constants $b_{p,q}$ as,

$$\begin{aligned}
&\forall q \in \{1, \dots, n\} \\
a_q &= \mathbb{E}_{(\mathbf{x}, y)} [(y - \alpha(\mathbf{x})) \beta_{q,q}(\mathbf{x})] \text{ \& } \{b_{p,q} := \mathbb{E}_{(\mathbf{x}, y)} [\beta_{q,q}(\mathbf{x}) \beta_{p,p}(\mathbf{x})] \mid p = 1, \dots, n\}
\end{aligned}$$

Then the ODE system can be re-written as $\forall q \in \{1, \dots, n\}$,

$$\frac{1}{\theta d} \cdot \frac{dw_q(t)}{dt} = a_q \cdot w_q(t)^{d-1} - \left(\sum_{p=1}^n b_{p,q} \cdot w_p(t)^d \right) \cdot w_q(t)^{d-1}$$

which can be rearranged to,

$$\frac{dw_q(t)}{a_q \cdot w_q(t)^{d-1} - \left(\sum_{p=1}^n b_{p,q} \cdot w_p(t)^d \right) \cdot w_q(t)^{d-1}} = \theta \cdot d \cdot dt \tag{33}$$

B.2.0.1 Our assumption can be written as : $b_{p,q} = b_q \delta_{p,q}$ for some constants $b_q, q = 1, \dots, n$: Then the above ODE reduces to,

$$\begin{aligned}
&\forall q \in \{1, \dots, n\} \\
\implies \frac{dw_q(t)}{a_q \cdot w_q(t)^{d-1} - b_q \cdot w_q(t)^{2d-1}} &= \theta \cdot d \cdot dt
\end{aligned} \tag{34}$$

B.2.0.2 Now we invoke the assumption that : $d = 2$ and $a_q > 0$ & $w_q(0)^2 \in (0, \frac{a_q}{b_q}) \forall q \in \{1, \dots, n\}$: Then the ODEs can be exactly integrated as follows,

$$\begin{aligned}
 & \forall q \in \{1, \dots, n\} \\
 & \implies \int_{w_q(0)}^{w_q(t)} \frac{dw_q(t)}{a_q \cdot w_q(t) - b_q \cdot w_q(t)^2} = 2\theta t \\
 & \implies \frac{1}{2a_q} \cdot \left[\log \frac{w_q(t)^2}{a_q - b_q w_q(t)^2} - \log \frac{w_q(0)^2}{a_q - b_q w_q(0)^2} \right] = 2\theta t \\
 & \implies w_q^2(t) = \frac{a_q}{b_q + \left\{ -b_q + \frac{a_q}{w_q^2(0)} \right\} e^{-4\theta a_q t}}
 \end{aligned} \tag{35}$$

Note that in the intermediate steps above we need $0 < w_q(t)^2, w_q(0)^2 < \frac{a_q}{b_q}$ for the logarithms to be well defined. And $w_q(t)^2 < \frac{a_q}{b_q}$ is ensured for the solution if we have $a_q > 0$ & $-b_q + \frac{a_q}{w_q^2(0)} > 0 \Leftrightarrow w_q(0)^2 < \frac{a_q}{b_q}$ and both of these are ensured by the assumptions.

Now for this case of $W = \text{diag}(\mathbf{w}) \in \mathbb{R}^{n \times n}$ & $d = 2$, equation 30 along with the ODE solution given above yields the following expression as claimed in the theorem statement,

$$\lim_{\eta \rightarrow 0} [S_{\text{rel}}]_{\mathbf{x}', \mathbf{x}} = \frac{|\sum_{r=1}^n \beta_{r,r}(\mathbf{x}') \beta_{r,r}(\mathbf{x}) \cdot w_{r,t}^2|}{|\sum_{r=1}^n \beta_{r,r}(\mathbf{x})^2 \cdot w_{r,t}^2|} = \frac{\left| \sum_{r=1}^n \frac{a_r \beta_{r,r}(\mathbf{x}') \beta_{r,r}(\mathbf{x})}{b_r + \left\{ -b_r + \frac{a_r}{w_r^2(0)} \right\} e^{-4\theta a_r t}} \right|}{\left| \sum_{r=1}^n \frac{a_r \beta_{r,r}(\mathbf{x})^2}{b_r + \left\{ -b_r + \frac{a_r}{w_r^2(0)} \right\} e^{-4\theta a_r t}} \right|} \tag{36}$$

□

B.3 Proof of Theorem 5.3

Proof. Define,

$$\begin{aligned}
 k_1 &:= \frac{\beta_{1,1}(\mathbf{x}') \beta_{1,1}(\mathbf{x})}{\beta_{1,1}(\mathbf{x}') \beta_{1,1}(\mathbf{x}) + \beta_{2,2}(\mathbf{x}') \beta_{2,2}(\mathbf{x})} \\
 k_2 &:= \frac{\beta_{1,1}(\mathbf{x})^2}{\beta_{1,1}(\mathbf{x})^2 + \beta_{2,2}(\mathbf{x}')^2}
 \end{aligned}$$

Then we can simplify equation 36 in this case to get,

$$\lim_{\eta \rightarrow 0} [S_{\text{rel}}]_{\mathbf{x}', \mathbf{x}} = \frac{|\beta_{1,1}(\mathbf{x}') \beta_{1,1}(\mathbf{x}) + \beta_{2,2}(\mathbf{x}') \beta_{2,2}(\mathbf{x})|}{|\beta_{1,1}(\mathbf{x})^2 + \beta_{2,2}(\mathbf{x}')^2|} \cdot \frac{|\alpha^2 + \beta^2 (k_1 e^{-4a_2 \theta t} + (1 - k_1) e^{-4a_1 \theta t})|}{|\alpha^2 + \beta^2 (k_2 e^{-4a_2 \theta t} + (1 - k_2) e^{-4a_1 \theta t})|} \tag{37}$$

Note that $k_2 \geq 0$ and hence $\beta^2 k_2$ can be mapped to the parameter b_2 in Lemma B.1. Also either k_1 or $1 - k_1$ is always non-negative and hence that one multiplied with β^2 maps to the parameter b_1 in Lemma B.1. Since $a_1, a_2 > 0$ and $\theta > 0$, the parameters p and q in Lemma B.1 get identified and we can invoke the lemma to realize that $\exists t_1^*, t_2^* > 0$ s.t for all $t \in [\max\{t_1^*, t_2^*\}, \infty)$ we have,

$$0 < \frac{|\beta_{1,1}(\mathbf{x}') \beta_{1,1}(\mathbf{x}) + \beta_{2,2}(\mathbf{x}') \beta_{2,2}(\mathbf{x})|}{|\beta_{1,1}(\mathbf{x})^2 + \beta_{2,2}(\mathbf{x}')^2|} \cdot \frac{\alpha^2 - |b_1| e^{-q^2 t^*}}{\alpha^2 + |b_2| e^{-p^2 t} + \beta^2 e^{-q^2 t}} \leq \lim_{\eta \rightarrow 0} [S_{\text{rel}}]_{\mathbf{x}', \mathbf{x}} \tag{38}$$

In above we have used the assumption that the lowerbound coming from Lemma B.1 is strictly above 0 and also the assumption about the first factor on the RHS of equation 37 being strictly above 0. Hence for gradient flow on squared loss on the predictor class given in equation 16, $\lim_{\eta \rightarrow 0} [S_{\text{rel}}]_{\mathbf{x}', \mathbf{x}}$ is s.t it can't decrease below a certain constant for all times beyond a certain initial time interval. □

Lemma B.1. Let,

$$f(t) := \frac{|\alpha^2 + b_1 e^{-p^2 t} + c_1 e^{-q^2 t}|}{|\alpha^2 + b_2 e^{-p^2 t} + c_2 e^{-q^2 t}|}$$

Suppose $t_1^* > 0$ is s.t $\forall t > t_1^*$ we have, $0 < \alpha^2 + b_2 e^{-p^2 t} + c_2 e^{-q^2 t}$

Suppose $t_2^* > 0$ is s.t $\forall t > t_2^*$ we have, $0 < \alpha^2 - b_1 e^{-q^2 t_2^*}$

Suppose $b_1, b_2 \geq 0$ and $\exists \beta \in \mathbb{R}$ s.t $b_1 + c_1 = b_2 + c_2 = \beta^2$

Then we have for all $t \in [\max\{t_1^*, t_2^*\}, \infty)$,

$$\frac{\alpha^2 - |b_1| e^{-q^2 t_2^*}}{\alpha^2 + |b_2| e^{-p^2 t} + \beta^2 e^{-q^2 t}} \leq \mathbf{f}(t)$$

Remark. Note that because $\alpha^2 > 0$ the above t_1^* & t_2^* always exists.

Proof. So we have for all $t \in [t_1^*, \infty)$,

$$0 < \alpha^2 + b_2 e^{-p^2 t} + c_2 e^{-q^2 t} = \alpha^2 + |b_2| e^{-p^2 t} + (\beta^2 - |b_2|) e^{-q^2 t} < \alpha^2 + |b_2| e^{-p^2 t} + \beta^2 e^{-q^2 t} \quad (39)$$

Similarly we have for all $t \in [t_2^*, \infty)$,

$$\alpha^2 + b_1 e^{-p^2 t} + c_1 e^{-q^2 t} = \alpha^2 + |b_1| (e^{-p^2 t} - e^{-q^2 t}) + \beta^2 e^{-q^2 t} \geq (\alpha^2 - |b_1| e^{-q^2 t_2^*}) > 0$$

Hence combining the above for all $t \in [\max\{t_1^*, t_2^*\}, \infty)$ we have the required inequality. □

APPENDIX C

ADDITIONAL EXPERIMENTS

C.1 A Study of Smoothed S_{rel} on CIFAR-100

CIFAR-100 is a labeled subset of the 80 million tiny images dataset. It consists of 100 classes and 20 super-classes. Thus, each image has a coarse label and a fine label and in this paper, we only use the latter. There are 500 training images and 100 testing images per class.

For this experiment train a ResNet-18 architecture, composed with a soft-max layer using the cross-entropy loss, on the CIFAR-100 training data and identify the top-3 classes with the highest class-wise accuracy. We then train a new ResNet-18 model⁴, again with softmax and the cross-entropy loss, on these top-3 classes. We choose $k = 20$ training data from each class and track the smoothed version of S_{rel} i.e $S_{\text{rel}}^{k, \text{smooth}}$ as given in Definition 3 for all the 9 possible class pairs. Some further details of the experimental setup are as follows in the table,

Parameter	Value
Depth of ResNet	18 (no batch norm)
The map that the f_{NN} implements	$\mathbb{R}^{3 \times 32 \times 32} \rightarrow \mathbb{R}^{10}$
Optimizer	ADAM
Learning rate	$1 \cdot 10^{-4}$
Mini-batch size	25
Dropout or any other regularization	Not Used
Top 3 classes for CIFAR-100	motorcycle, orange, wardrobe

In Figure 13 we see the time evolution of smoothed S_{rel} for all the 9 possible class pairs corresponding to images from the classes, $\{\text{plane}, \text{car}, \text{ship}\}$. The plots show the mean S_{rel} value (averaged over 5 random runs) for each class pair as well as the standard deviation. Again, we observe that for all pairs, the intra-class S_{rel} value is higher than the inter-class S_{rel} value and, while the intra-class S_{rel} value remains relatively constant through the training process, the inter-class S_{rel} value progressively decreases as training progresses.

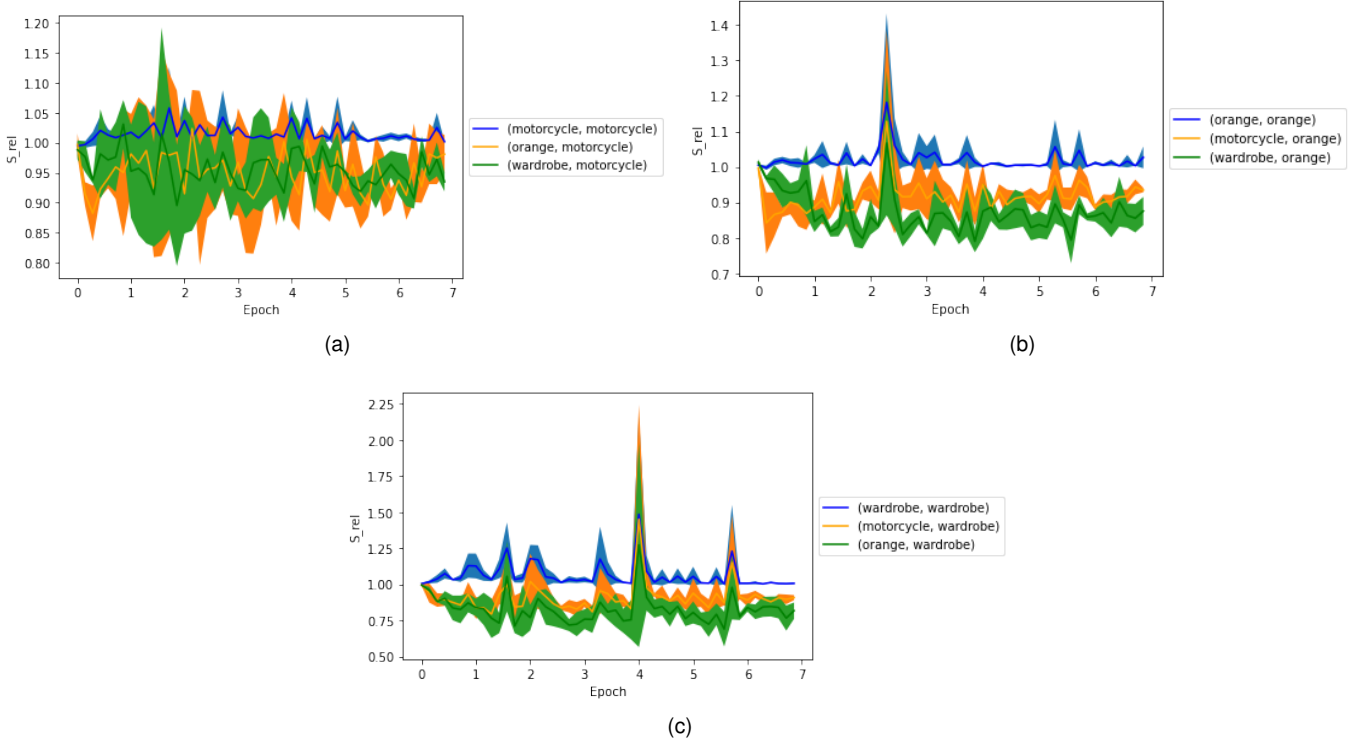


Fig. 13. $S_{\text{rel}}^{\text{smooth}}$'s time evolution for the two image classes being chosen from $\{\text{motorcycle}, \text{orange}, \text{wardrobe}\}$ with Class-x being motorcycle in (a), orange in (b) and wardrobe in (c)

C.2 Other Experimental Details

The experiments were run on the Colab GPU and a NVIDIA 11 GB GPU. The training time for each run (7 epochs) is less than an hour and the ResNet-18 (without batch norm) achieves 87, 78, 94% accuracies respectively on SVHN, CIFAR-10, 100.

⁴. Again, we remove batch-normalization from the ResNet-18 model, for gradient updates with mini-batch size 1 which is necessary to define \mathbf{w}_t^+ in Definition 2 and Definition 3.